Ain Shams Engineering Journal 15 (2024) 102390

Contents lists available at ScienceDirect

Ain Shams Engineering Journal

journal homepage: www.sciencedirect.com

Impact of chimney divergence and sloped absorber on energy efficacy of a solar chimney power plant (SCPP)

Dipak Kumar Mandal [a], Nirmalendu Biswas [b], Nirmal K. Manna [c], Ali Cemal Benim [d,*]

[a] Department of Mechanical Engineering, College of Engineering and Management, Kolaghat 721171, India
[b] Department of Power Engineering, Jadavpur University, Salt Lake, Kolkata 700106, India
[c] Department of Mechanical Engineering, Jadavpur University, Kolkata 700032, India
[d] Department of Mechanical and Process Engineering, Düsseldorf University of Applied Sciences, Germany

ARTICLE INFO

Keywords:
Solar chimney power plant (SCPP)
Chimney divergence angle
Sloped absorber surface
Power generation
Efficiency
Regression analysis

ABSTRACT

A numerical study is carried out meticulously to scrutinize the impact of different shapes of chimneys like circular (outer dia, d_c), convergent (outer dia, $0.5d_c$), divergent (outer dia, $1.5d_c$), sudden contraction (outer dia, $0.5d_c$), and sudden expansion (outer dia, $1.5d_c$) on the performance of an SCPP. Furthermore, the parametric impact with different chimney divergence angles (CDA, ϕ), and ground absorber slope angle (GSA, γ) on the SCPP performance is also scrutinized. Optimum divergence angle ($\phi = +0.75^{\circ}$) enhances the power generation up to ~ 47% (76 kW) with a horizontal ground absorber surface. An increase or decrease in CDA lessens the power generation. With a sloped ground absorber angle $\gamma = 0.6^{\circ}$, the gain in power generation is 60% (82 kW). The study of combination of ground sloped absorber ($\gamma = 0.6^{\circ}$) and divergent chimney ($\phi = +0.75^{\circ}$) shows enhancement of the power generation upto 80% (92 kW) more than the classical Manzaranes plant.

1. Introduction

It is pragmatic that fossil fuels are limited, polluting our environment, threatening life on our planet, and hence need to be restrained. This whole framework needs progress in clean or sustainable energy. A solar thermal power plant (SCPP) is one of the favorable potentials for using solar energy for large-scale power generation.

SCPP comprises three major components, collector, ground absorber, and chimney. A collector is a transparent cover for passing solar radiation through it. This should be anti-reflexing in nature to lessen the loss. Solar energy after passing through the collector gets absorbed by the ground and heats the air. The ground is having high thermal conductivity and it is painted with black color. The chimney is the central unit used for updraft caused by heated air in-between collector and ground. The chimney enables natural convection circulation from the collector inlet to the exit of the chimney. A wind turbine is placed near the chimney base in order to use flow energy into kinetic energy that in turn produces electrical power by generator [39,33,16]. This process has been described in a flow chart, as in Fig. 1.

The theory of solar chimney power plants was initiated in the early 1900 s. The first large-scale SCPP was made in Manazaranes, Spain in 1982 by Haaf et al. [23,24] . Its size, collector radius of 122 m, collector inlet of 1.85 m, chimney diameter, and height are 10.16 m and 194.6 m respectively in order to generate ~ 50 kW power. Because of the chimney and collector, its installation cost is very high. Power conversion efficiency is also very low. To overcome these difficulties, researchers have proposed some novel ideas in order to performance enhancement. The selection of proper geometry might be one alternative solution.

For a fixed chimney height, the shape of the chimney enables the performance of the plant. Power and efficiency both could be enhanced by tapering the chimney at the top as reported [38]. On the contrary, [8] has reported no improvement in performance with convergent chimneys. However, an increase in the area ratio of chimneys augments static pressure, as examined by [50]. Koonsrisuk and Chitsomboon [29] in their numerical study, they have claimed improvement of velocity, mass flow rate (4.5 times) power (94.29 times) for 16 m chimney outer diameter (inlet diameter is 4 m). Compared to conventional plant sloping collectors divergent chimney SCPP produces 100 times more power, as reported by Koonsrisuk and Chitsomboon [29]. Since they have claimed their results by one data, hence further simulation is required to support this. The computational study by Patel et al. [37] showed an optimum divergence angle of 2° in order to have the best

* Corresponding author at: Department of Mechanical and Process Engineering, Düsseldorf University of Applied Sciences, Germany
E-mail addresses: dipkuma@yahoo.com (D. Kumar Mandal), biswas.nirmalendu@gmail.com (N. Biswas), nirmalkmannaju@gmail.com (N.K. Manna), alicemal.benim@hs-duesseldorf.de (A.C. Benim).

https://doi.org/10.1016/j.asej.2023.102390
Received 5 January 2023; Accepted 17 July 2023
Available online 26 July 2023

Nomenclature

A_i	air inlet area, m^2
A_{ch}	chimney area, m^2
A_{coll}	area of collector, m^2
c_p	specific heat of air, kJ/kgK
d_c	chimney diameter, m
h_i	inlet height of collector
d_g	diameter of ground, m
h_c	chimney height, m
g	gravitational acceleration, m/s^2
Gr	Grashof number
I	solar irradiation, W/m^2
L	characteristic length, m
m_a	mass flow rate, kg/s
p	pressure, Pa
Pr	Prandtl number
Q	volume flow rate at chimney base, m^3/s
Ra	fluid Rayleigh number
RNG	renormalization group
T_a	ambient temperature, K
T_{CB}	chimney inlet temperature, K
V_{ch}	velocity through chimney, m/s
P_{act}	electrical power developed by generator, W
u_i	velocity vector, m/s

Greek symbols

α	thermal diffusivity, m^2/s
β	thermal expansion coefficient, 1/K
γ	ground slope angle
φ	chimney divergence angle
μ	dynamic viscosity, kg/ms
ν	kinematic viscosity, m^2/s
η_c	collector efficiency, %
η_o	overall efficiency, %
ρ_{air}	density of ambient air, kg/m^3

Subscripts

ch	chimney
CB	chimney base
eff	efficiency
in	inlet
o	overall
out	outlet
max	maximum

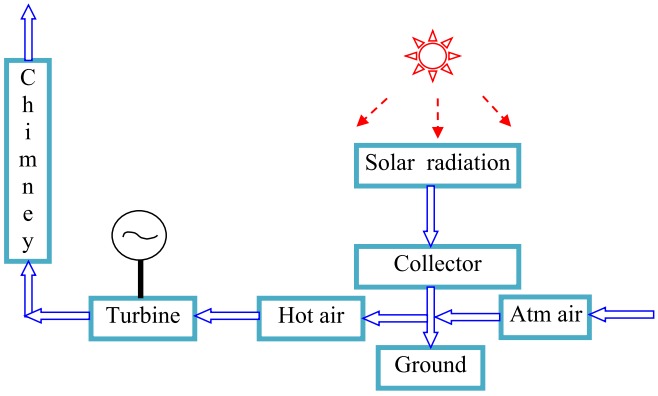

Fig. 1. Overall processes of solar chimney power plant (SCPP).

performance. Improvement of power (2.6–3 times) could be obtained by diffuser tower [35]. For the same dimension of Manzaranes plant, 1° of chimney slope shows the velocity rise from 9.1 m/s to 11.6 m/s, power rise of 108% as simulated by Hassan et al. [25]. Calculated power is made by 0.5 × density × area × (velocity)^3. On the contrary, a similar study by [13] for the Manzanares plant shows more than 300% power augmentation for diverging chimneys (for an area ratio of 16). This high power generation may be calculated by using maximum minimum static pressure. Das and Chandramohan [15] have reported 2° divergence angle is optimum to achieve maximum power, gaining in power about 280% compared to the cylindrical chimney in a small model numerically. The previously mentioned discussion summarizes that most of the researchers agreed with the rise of performance for the divergent chimney but the optimum divergence is different and the performance is the function of different geometry of SCPP. The effect of the system geometry with a curved junction at the entry to chimney on the heat transfer process and the fluid flow in the system has been investigated by Tayebi and Djezzar [46–47].

The ground slope may be another parameter for designing SCPP in order to enhance performance. Unfortunately, a few researchers [11,12] have scrutinized this phenomena considering the Manzanares plant. In one work, they have taken the slope starting from 5 m after the inlet, and another 21 m after the inlet. So far, no work has been found where the slope starts from the collector inlet. Combination with a wavy structure which is frequently encountered in small-scale convective devices [4] has also not been investigated so far. However, [11] have noted a 34.1% enhancement in velocity and 66% enhancement in power. [12] have reported 0.5° slope results in maximum velocity and power, which is about a rise 17.75% power and 37% in velocity. From the entropy generation analysis of convective airflow in a solar updraft tower power, Tayebi [49] has observed that chimney section is the main location of higher irreversibility.

Since the Manzanares plant is one the well-known plant, which attracted many researchers, consequently many efforts are made to improve its performance. The performance by altering chimney height and diameter [9,18,31,44,51], and how it affects the performance of SCPP, it shows rise in the power for increasing chimney height. The optimal height is different for different plants, this height may be raised proportionally with collector diameter [51]. Tayebi and Djezzar [48] demonstrated that the temperature and velocity of fluid increases with lessening the collector radius. The effect of collector diameter and its slope is studied [6,10,21,25,28,31]. Power generates more for the sloped collector, while it has some limitations also. The roughness of the transparent collector is also studied in order to find out the benefit to the performance of the plant [19,17]. Some studies on heat storage [3], variation in radiation and realistic model [22,20,26], using fillet at the chimney inlet [36], and 2D numerical study [40,41,42] has been observed by using Manzanares plant also.

The vast pool of literature clearly demonstrates the use of the Manzanares plant for generating power utilizing solar energy. In this study, an attempt has been made to maximize the thermal performance and to enhance the power generation of a solar chimney power plant (SCPP) of Manzaranes unit by modifying the geometry. This exercise is carried out by adopting different chimney shapes (convergent, divergent, sudden expansion, sudden contraction) along with the ground sloped absorber. This study aims to scrutinize the impact of divergence angle of the chimney, ground slope of absorber and combined effect for a ground sloped divergent chimney SCPP in case of the Manzaranes plant. Motivation from the previously mentioned studies yields some certain contradicting results in the divergence chimney and thereby the impact of

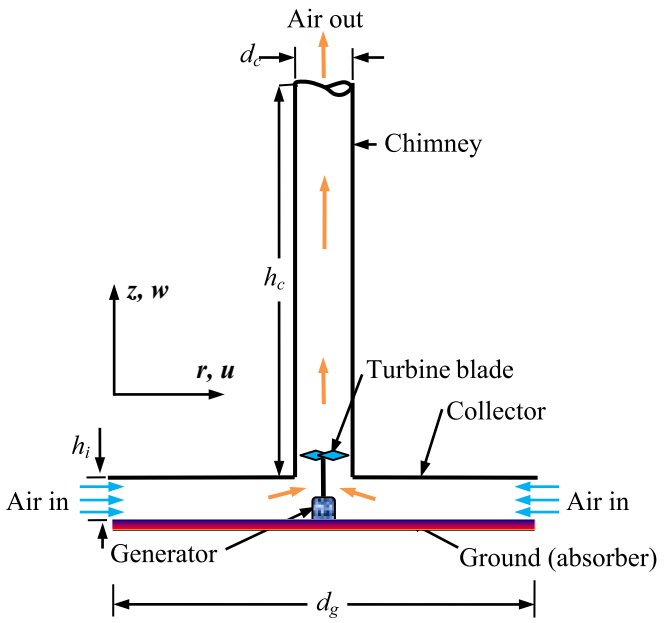

Fig. 2. Computational domain of SCPP with the horizontal ground and cylindrical chimney.

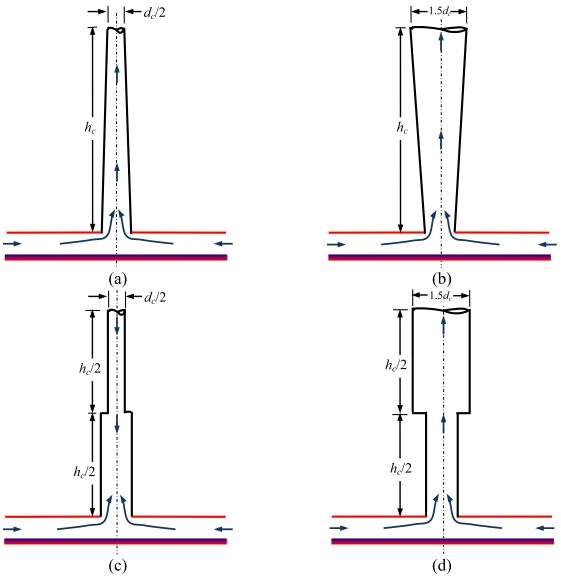

Fig. 3. Different configurations of the modified SCPP model (cross-sectional view) with different chimney shapes: a) convergent, b) divergent, c) sudden contraction, and d) sudden expansion.

divergence is studied. As far as the ground absorber slope is concerned, a very few studies have addressed the effect of ground absorber slope, although no one has considered the ground absorber slope from the inlet of the collector. We, the researchers first adopted the concept of the above. It is also noteworthy that no one has studied ground sloped absorber surface along with divergent chimney together in a SCPP towards the improvement of performance. In this background, the present work contributes novelty a lot to the research community. Flow and heat transfer analysis along with performance analysis is carried out in detail for all the models by pressure, temperature, velocity, rate of mass flow, power generation, collector efficiency, and overall efficiency. In the present study the chimney divergence angle, (CDA) and ground slope angle (GSA), are varied as $\phi = -0.75,\ 0,\ +0.75,\ 1.5,\ 2.25,\ 3.0^{\circ}$ and $\gamma = 0,\ 0.12,\ 0.24,\ 0.36,\ 0.48,\ 0.6^{\circ}$, respectively.

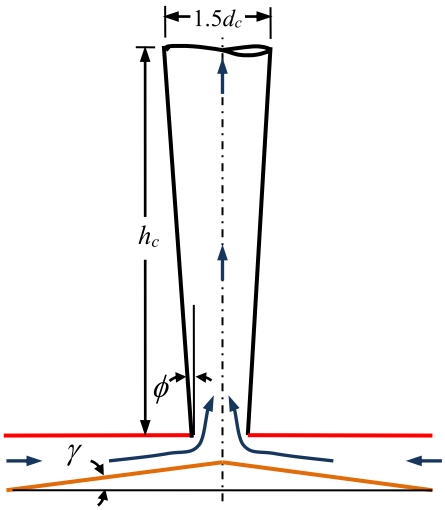

Fig. 4. Ground sloped absorber surface along with divergent chimney-based SCPP model.

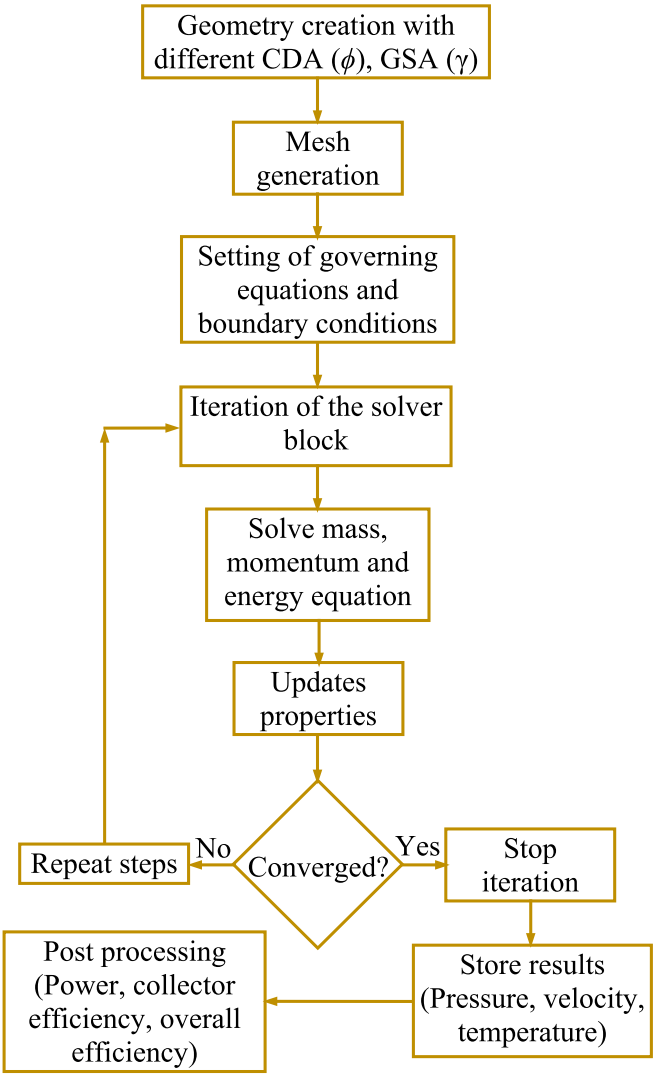

Fig. 5. Solution algorithm of the solver in ANSYS Fluent.

Table 1
Details of solution method and controlling parameters in ANSYS Fluent. [14,36,12].

Criteria	Settings
Scheme:	SIMPLE
Discretization technique:	Gradient: Green Gauss cell-based
	Pressure: PRESTO
	Momentum: Second order upwind
	Turbulent kinetic energy: Second order upwind
	Turbulent dissipation rate: First order upwind
	Energy: Second order upwind
	Discrete ordinates: First order upwind
Under relaxation factor:	Pressure: 0.3
	Momentum: 0.8
	Turbulent kinetic energy: 0.8
	Turbulent dissipation rate: 0.8

Table 2
Boundary conditions for the computational model [28].

Boundary	Conditions	Magnitudes
Collector	Semitransparent, glass	$h = 10$ W/m^{2}K, $T = 302$ K
Absorber	Opaque wall	$q = 0$ W/m^2
Chimney	Adiabatic wall	Heat flux, $q = 0$ W/m^2
Inlet	Pressure boundary	Zero gauge pressure, $T = 302$ K
Outlet	Pressure boundary	Zero gauge pressure

2. Methodology and analysis

2.1. Formation of physical domain

For this study, the Manzanares plant [23] is chosen as the base model as shown in Fig. 2. This has a horizontal ground absorber surface (with diameter $d_g = 244$ m), collector inlet height ($h_i = 1.85$ m), chimney height ($h_c = 194.6$ m), and chimney diameter ($d_c = 10.16$ m). In order to enhance the performance of a SCPP, a parametric analysis is carried out by modifying the shape of the chimney of a classical SCPP. Four different shapes of the chimney are taken into consideration as a) convergent, b) divergent, c) sudden contraction, and d) sudden expansion as given in Fig. 3. For further improvement of performance, this study is extended to scrutinize the influence of sloped ground absorber surface, impact of the chimney divergence, and their combine effect as shown in Fig. 4. For the cylindrical chimney, chimney divergence angle (CDA, $\phi = 0^{\circ}$), and horizontal ground model, no ground absorber slope angle (GSA, $\gamma = 0^{\circ}$) are varied to obtain the best model performance.

For analysis of the modified SCPP model, it is assumed that the working fluid (air with Pr = 0.71) is incompressible [27]. There is no change in the environmental conditions surrounding the SCPP. In fact, heat loss from the chimney is negligible and the Boussinesq approximation $(\rho - \rho_a)g \approx -\rho_a\beta(T - T_a)$ is valid for taking care of the density variation. In this analysis, constant solar radiation of 1000 W/m^2 is considered during each process. Thermophysical properties of working fluid are assumed constant [36,28].

Changes in potential and kinetic energy are ignored [15,36].

2.2. Governing equations and modeling

2.2.1. Flow modeling

The performance analysis of the modified SCPP is carried out numerically by solving the mass, momentum, and energy conservation equations with appropriate boundary conditions. The constitutive equations [28] are expressed in the tensor form (where the indices i and j correspond to 1, 2, and 3, respectively) as.

Continuity equation

$$\frac{\partial}{\partial x_i}(\rho u_i) = 0 \tag{1}$$

Table 3
Thermophysical properties of air, collector, ground, and chimney (at ambient conditions) (Cuce *et al.*, [9]).

Thermophysical properties	Air	Collector	Absorber	Chimney
Material	–	Glass	–	Aluminum
Thickness	–	0.004	0.5	0.00125
Emissivity	–	0.1	0.9	1.0
Absorptivity	–	0.03	0.9	0
Trasmissivity	–	0.9	Opaque	Opaque
Refractive index	–	1.526	1.0	1.0
Density (ρ) kg/m^3	1.2046	2500	2160	2100
Specific heat (C_p) J/kg/K	1006.43	750	710	880
Thermal conductivity (K), W/mK	0.0259	1.15	1.83	1.4
Thermal expansion coefficient (β), K^{-1}	0.00331	–	–	–

Table 4
Mesh sensitivity test with different mesh sizes using the chimney base velocity and temperature, and mass flow rate.

Parameters checked	Element size			
	0.90	0.85	0.80	0.75
Mesh size	53,883 (M_1)	62,021 (M_2)	73,862 (M_3)	85,551 (M_4)
CB velocity	10.04	10.63	10.57	10.60
% of change	–	5.8764	0.5644	0.2838
CB temperature	315.69	315.78	315.840	315.86
% of change	–	0.0285	0.0190	0.0063
Mass flow rate	32.79	32.11	31.970	31.91
% of change	–	2.0738	0.436	0.1876

Momentum equation

$$\frac{\partial}{\partial x_j}(\rho u_i u_j) = -\frac{\partial p}{\partial x_i} + \frac{\partial}{\partial x_j}\left[(\mu_t + \mu)\left(\frac{\partial u_i}{\partial x_j} + \frac{\partial u_j}{\partial x_i}\right) - \frac{2}{3}(\mu_t + \mu)\frac{\partial u_i}{\partial x_i}\delta_{ij}\right] + \rho g_i \beta \Delta T \tag{2}$$

Energy equation

$$\frac{\partial}{\partial x_j}(\rho u_i T) = \frac{\partial}{\partial x_j}\left[\left(\frac{\mu}{Pr} + \frac{\mu_t}{\sigma_t}\right)\frac{\partial T}{\partial x_j}\right] \tag{3}$$

where, Pr and σ_t correspond to the Prandtl number and turbulent Prandtl number. In Eq. (2), the term $\rho\beta g_i \Delta T$ is the buoyant force. Furthermore, the turbulent and laminar viscosity is expressed by the symbol μ_t and μ (in Ns/m^2), respectively, and the symbol δ is the Kronecker delta (where $\delta = 1$, when $i = j$ and else $\delta = 0$).

2.2.2. Turbulent flow modeling

Before conducting the extensive simulations, it is important to know the fluid flow regime (whether laminar or turbulent). To assesses this point, Rayleigh number (Ra) is calculated by $\mathrm{Ra} = \frac{g\beta\Delta TL^3}{\alpha\upsilon} = \mathrm{Gr} \times Pr$, where β is the thermal expansion coefficient $= 1/T_{max}$, $\Delta T = (T - T_0)$, T_0 is the operating temperature, L = characteristic length, α = thermal diffusivity $= \frac{k}{\rho C_p}$, υ = kinematic viscosity $= \mu/\rho$, Gr and Pr are the Grashof number and Prandtl number respectively. From the considered geometrical dimensions, the calculated value of Ra $\geq 10^9$, so the fluid flow domain is in the turbulent regime. Therefore, turbulent flow modeling is of utmost necessity. In the ANSYS-Fluent solver, there are three different types of turbulent models. Available literature tells most of the used models is RNG k-ε turbulent model and is more appropriate for strong swirl and vortex effects Hassan et al. [25], Gholamalizadeh and Kim [21], Sudprasert et al. [45,1,12], Keshari et al. [28,11], Gholamalizadeh and Kim [21].

The model equations for the RNG $k-\varepsilon$ turbulence [9,12] are given by

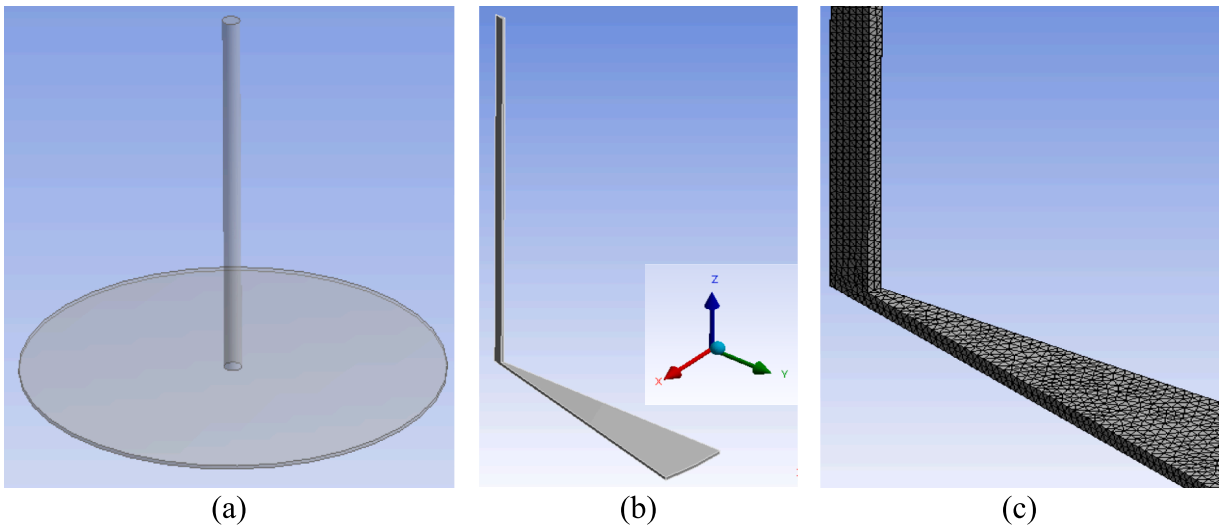

Fig. 6. Mesh structure used in the computational model for the modified SCPP: (a) 3D view of the SCPP model, (b) 15° CFD model with 3D coordinate system, and (c) enlarged view of the chimney base area.

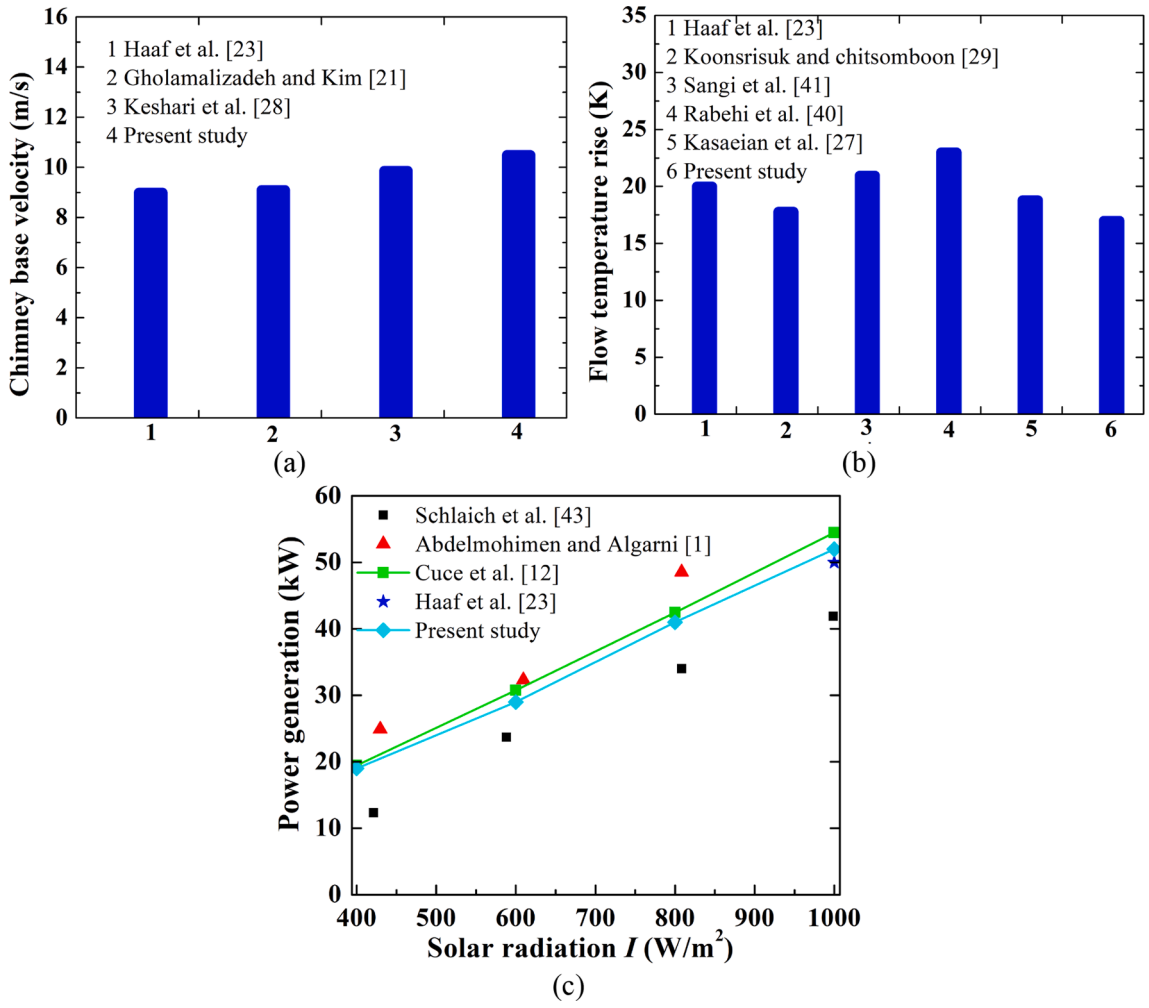

Fig. 7. Comparison of (a) chimney base velocities, (b) temperature rise, (c) power generation with published results.

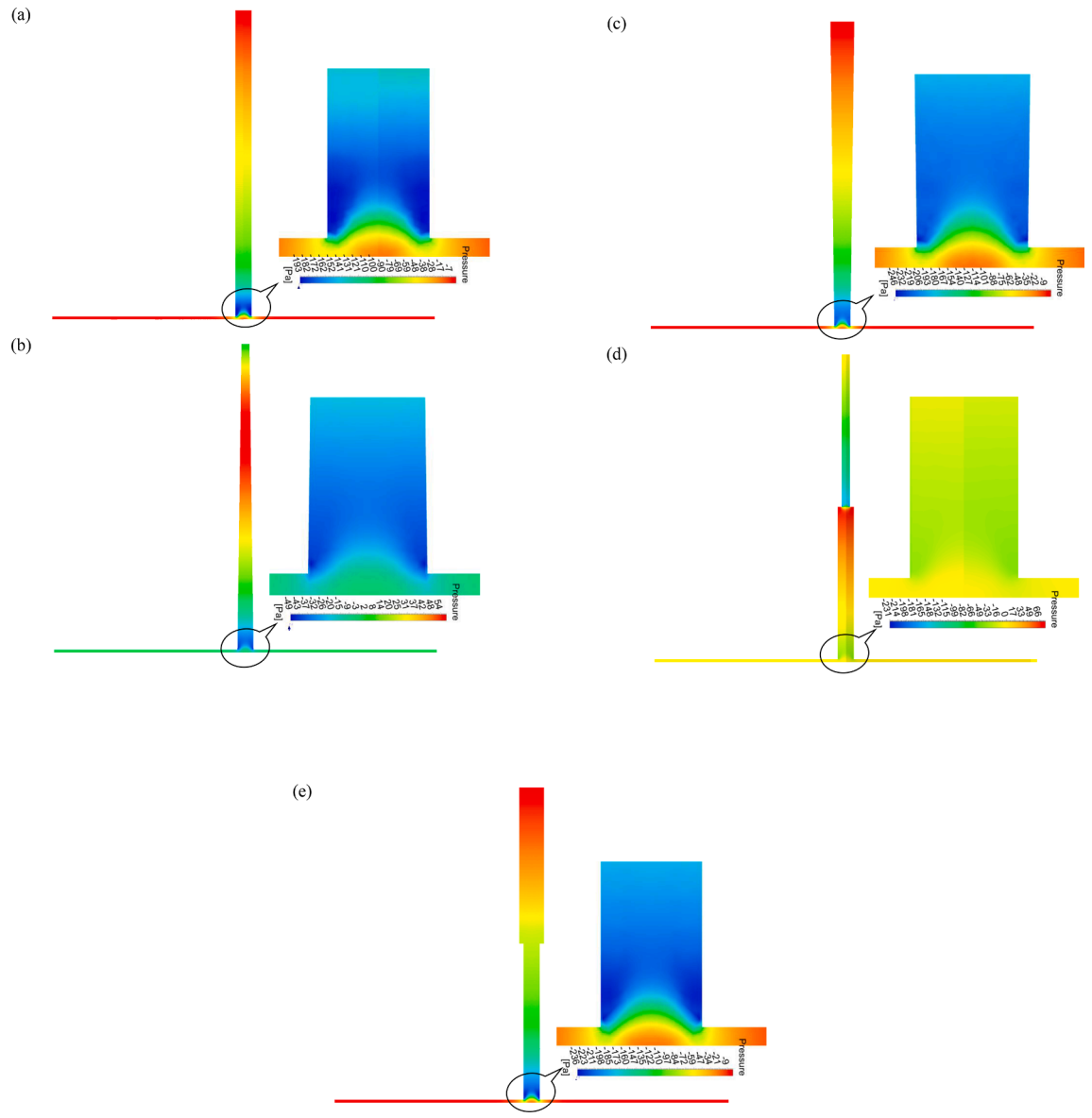

Fig. 8. Local pressure contour plots for the different shaped chimney: (a) cylindrical, (b) convergent, (c) divergent, (d) sudden contraction, and (e) sudden expansion.

$$\frac{\partial}{\partial x_i}(\rho k u_i) = \frac{\partial}{\partial x_j}\left[\alpha_k \mu_{eff}\frac{\partial k}{\partial x_j}\right] + G_k + G_b + \rho\varepsilon - Y_M + S_k \tag{4}$$

$$\frac{\partial}{\partial x_i}(\rho \varepsilon u_i) = \frac{\partial}{\partial x_j}\left[\alpha_\varepsilon \mu_{eff}\frac{\partial \varepsilon}{\partial x_j}\right] + C_{1\varepsilon}\frac{\varepsilon}{k}(G_k + C_{3\varepsilon}G_b) - C_{2\varepsilon}\rho\frac{\varepsilon^2}{k} - R_\varepsilon + S_\varepsilon \tag{5}$$

Turbulent kinetic energy production due to mean velocity gradient,

$$G_k = -\rho u_i u_j \frac{\partial u_i}{\partial u_j} \tag{6}$$

Turbulent kinetic energy production owing to buoyancy,

$$G_b = \beta g_i \frac{\mu_t}{Pr_t}\frac{\partial t}{\partial x_i} \tag{7}$$

The dissipation rate due to fluctuating dilatation in compressible turbulence,

$$Y_M = 2\rho\varepsilon M_t^2 \tag{8}$$

where M_t is the Mach number for turbulent flow.

The additional terms that differs from the standard model,

$$R_\varepsilon = \frac{C_\mu \rho \eta^3(1-\eta/\eta_0)}{1+\beta\eta^3}\frac{\varepsilon^2}{k} \tag{9}$$

In the aforesaid Eq. (9) the values of $\eta_0 = 4.38$, $\beta = 0.012$, $\eta = Sk/\varepsilon$[1].

2.2.3. Radiation modeling

Radiation modeling is done by ANSYS inbuilt function by Discrete ordinates (DO) model through a semitransparent collector as reported Fallah and Valipour [19], Abdelmohimen and Algarni [1,12], Keshari et al. [28,11], Das and Chandramohan [14].

The heat transfer equations [28],

$$\nabla.(I(\vec{r},\vec{s})\vec{s}) + (a+\sigma_s)I(\vec{r},\vec{s}) = an^2\frac{\sigma T^4}{\pi} + \frac{\sigma_s}{4\pi}\int_0^{4\pi} I(\vec{r},\vec{s}')\varpi(\vec{s}.\vec{s}')d\Omega' \tag{10}$$

where $\vec{s}'$ denotes scattering direction vector, a denotes absorption coefficient, n is the refractive index of the medium, σ_s is scattering coefficient, ϖ denotes phase function, Ω' is the solid angle, I is the radiation

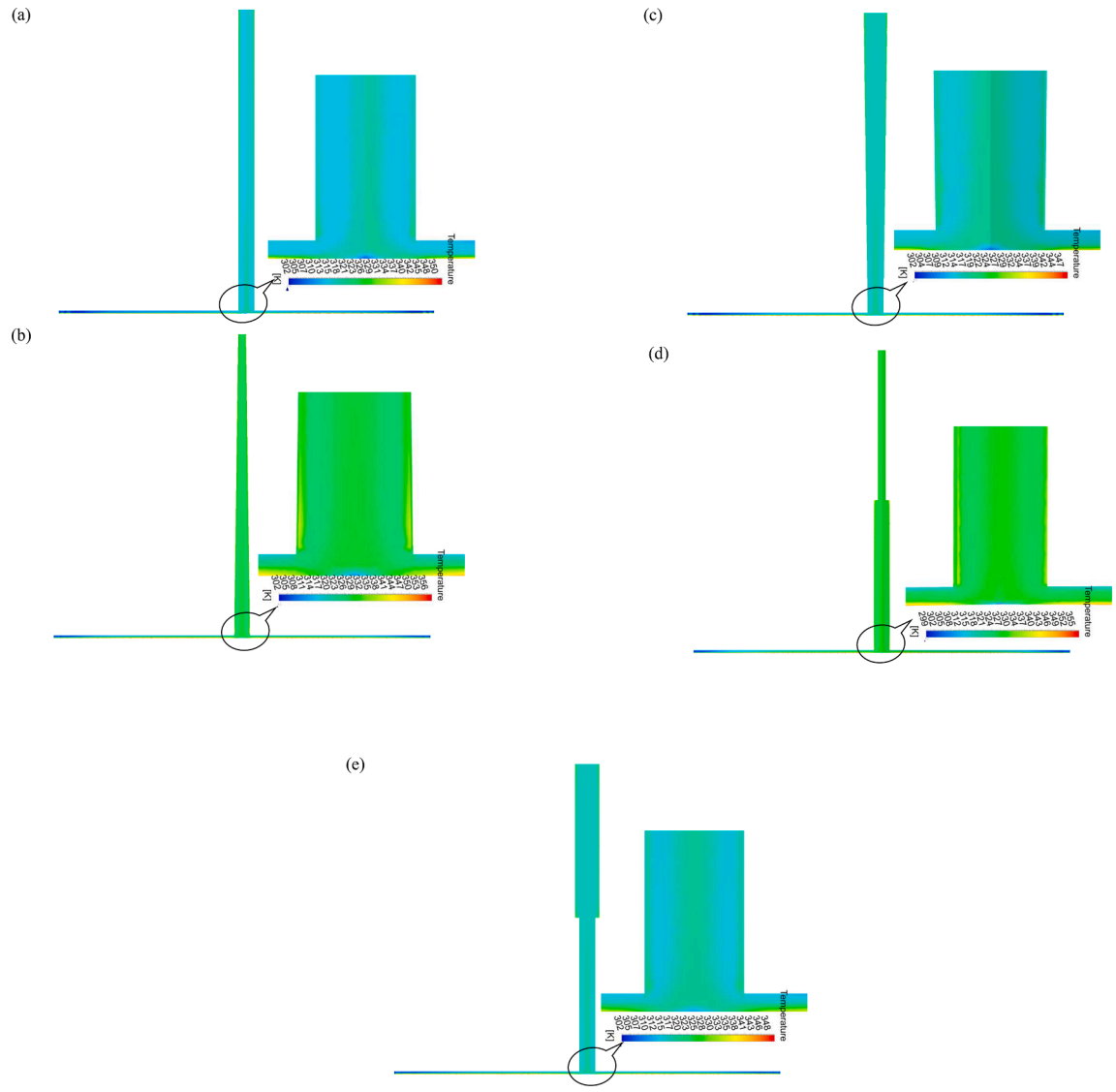

Fig. 9. Local temperature contour plots for the different shaped chimneys: (a) cylindrical, (b) convergent, (c) divergent, (d) sudden contraction, and (e) sudden expansion.

intensity in W/m^2 [2].

2.2.4. Estimation of performance parameters

The performance of the modified SCPP is scrutinized through generated actual power (P_{act}), collector efficiency (η_{coll}), chimney efficiency (η_{ch}), and overall efficiency (η_o). Actual power generation is calculated as [9,11,12,13].

$$P_{act} = \eta_t \times \Delta p \times Q \tag{11}$$

where η_t = turbine efficiency, taken 0.8 [28], Δp = pressure drop in the turbine = average pressure at the chimney base × pressure drop ratio (pressure drop ratio is taken to be 2/3, [30]).

Q = volume flow rate of air at the chimney base = area of the chimney × average velocity of air at chimney base.

$$\text{Collector Efficincy } (\eta_c) = \frac{\text{Heat utilized}}{\text{Energy available by radiation}} = \frac{m_a c_p (T_{CB} - T_a)}{A_{coll} \times I} \tag{12}$$

where,

m_a = mass flow rate of air at Chimney base in kg/s.

T_{CB} = air temperature at the chimney base.

A_{coll} = collector area.

I = irradiation

$$\text{Overall efficiency } (\eta_o) = \frac{\text{Power produced}}{\text{Energy available by radiation}} \tag{13}$$

3. Numerical procedure

3.1. Solution approach

An axisymmetric CFD model is prepared using the ANSYS-Fluent 18.1 solver through a workbench. Here, the 15° CFD model is done to reduce the total iteration period instead of the whole meshing. Many researchers like [25] have used the 180° CFD model, 90° CFD model is considered by Cuce *et al.* [12] , and 5° CFD model by Koonsrisuk and Chitsomboon, [29] for lessening the meshes. The SIMPLE algorithm method is applied for the solution and the subsequent procedure is illustrated by a flow chart (as in Fig. 5). For obtaining the converged solution, a minimum criterion of 10^6 is chosen for the computation [34,5,7,32]. Furthermore, the solution methods are detailed in Table 1.

The solar radiation level is used constantly at 1000 W/m^2 for this

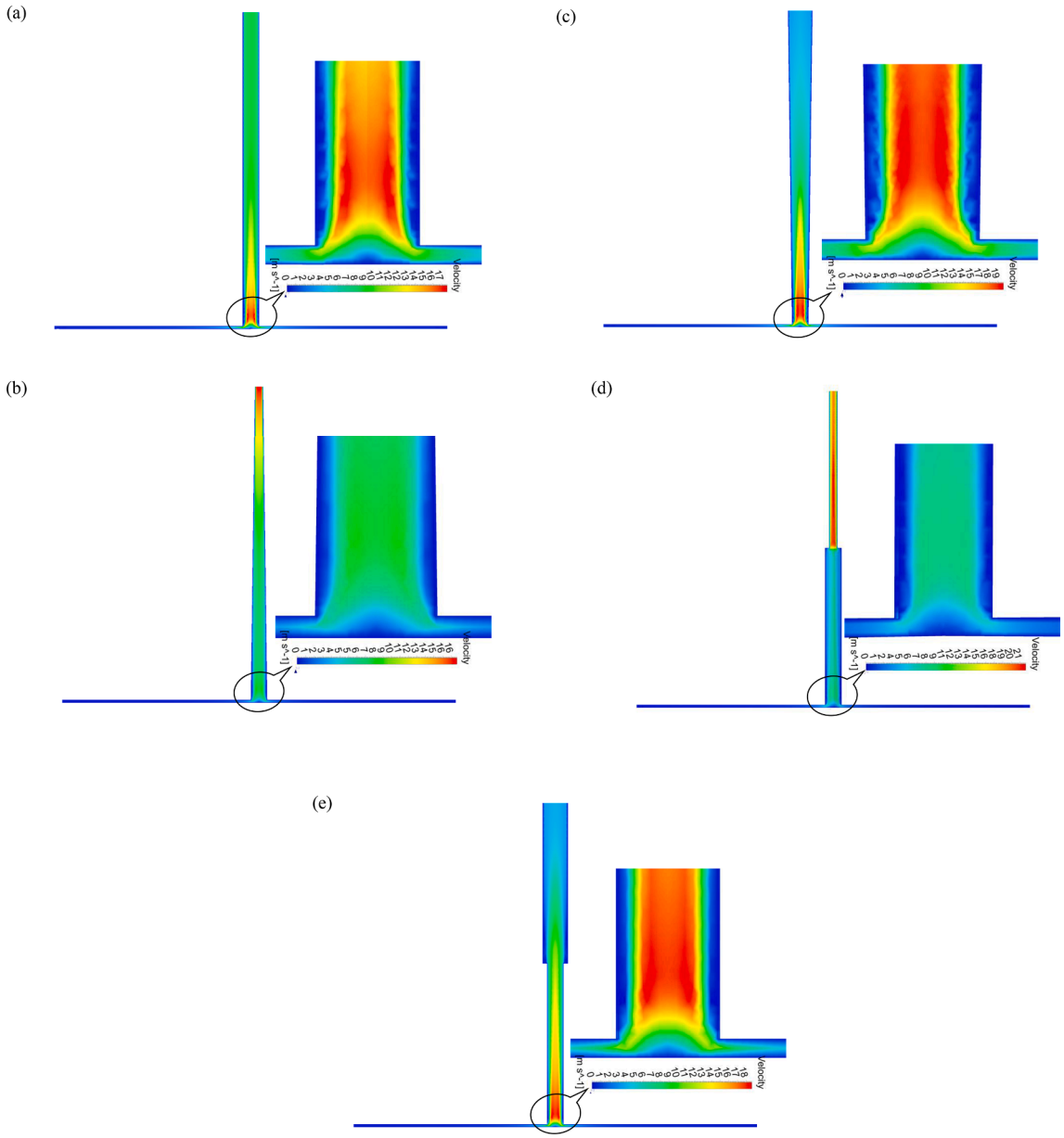

Fig. 10. Local velocity contour plots for the different shaped chimneys: (a) cylindrical, (b) convergent, (c) divergent, (d) sudden contraction, and (e) sudden expansion.

study. The topographical data of Manzaranes, Spain (latitude 38.99°N, longitude 3.37°W [23,24] is used to estimate the solar insolation and solar beam radiation by the solar calculator available in the ANSYS-Fluent solver. The different boundary conditions for the modified cases are presented in Table 2 [28]. Furthermore, Table 3 indicates the thermophysical properties along with the condition of the computational domain.

3.2. Meshing and mesh independence study

In order to capture the correct results of the computational domain, mesh independence for the modified SCPP is carried out. The mesh independence study is done by different grid sizes with different element sizes. The results are compared through the chimney base velocity, temperature, and mass flow rate. Different mesh size like M_1 (53883), M_2 (62021), M_3 (73862), M_4 (85551) for the element size 0.90, 0.85. 0.80. and 0.75 respectively are considered for the analysis, which is presented in Table 4. M_3 mesh size is used as the best mesh for the computational domain as the cumulative error in the consecutive grids changes are less. As the shape of the chimney changes due to the geometric modification and the ground absorber slope, the grid size is finalized by taking 0.8 element size for all the models. The details about the mesh structure used in the computational model for the modified SCPP are presented in Fig. 6 with (a) a 3D view of the SCPP model, (b) a 15° CFD model with a 3D coordinate system, and (c) enlarged view of the chimney base area.

3.3. Validation of present study

Before conducting the extensive simulation, the present solver is utilized for validating the published results. The validation study is conducted by the comparisons of chimney base velocity, temperature rise, and power produced in kW, as described in Fig. 7. The experimental-based works [23,43] are compared with the present solver results and it shows reasonably good accordance. Other predicted data from numerical study considering Manzaranes data are also compared

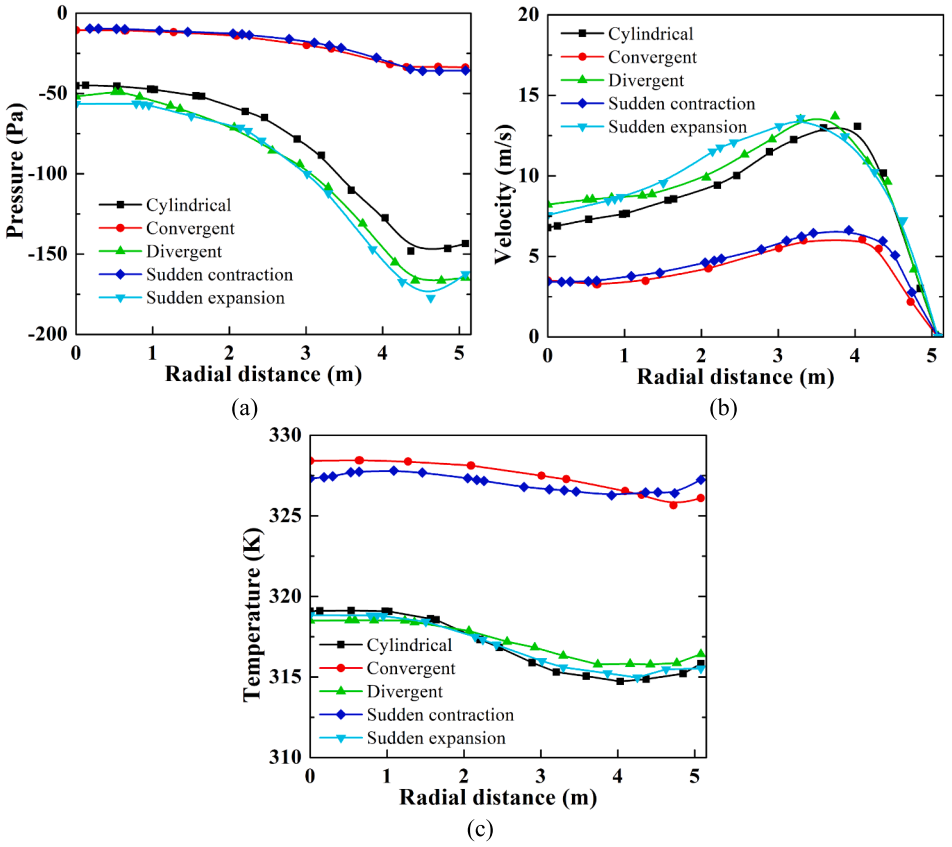

Fig. 11. Local variation of (a) pressure, (b) temperature, and (c) velocity distributions at the chimney base.

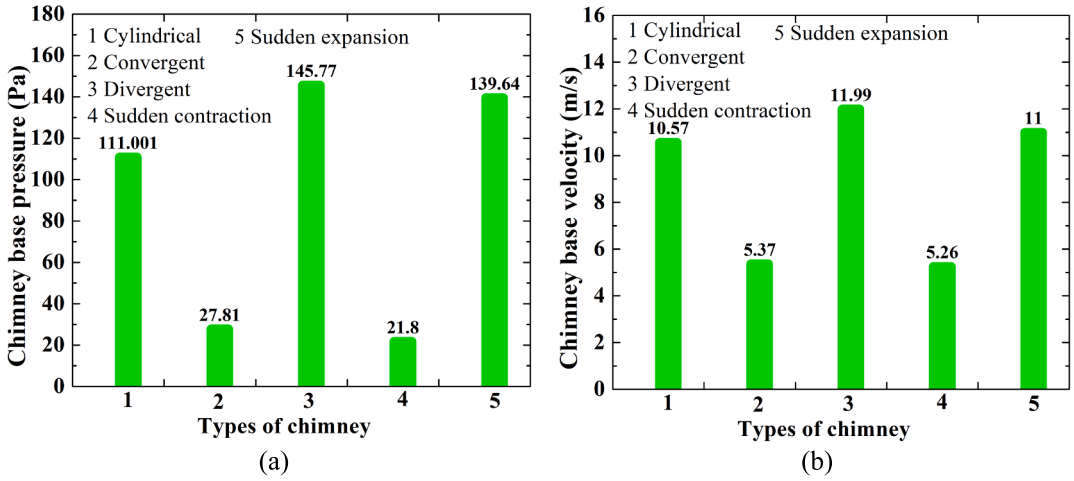

Fig. 12. Variation of chimney base (a) average pressure, and (b) velocity for cylindrical, convergent, divergent, sudden contraction, sudden expansion shaped chimneys.

and the comparison is in the acceptable range. This confirms the accuracy level of the present solver.

4. Analysis of results

In this work, an attempt has been taken to improve the performance of a classical SCPP of Manzaranes plant. Therefore, to understand the impact of different shapes of chimneys on the performance of a SCPP, in the first part of the study, a numerical analysis is performed for the various shapes of the chimney like circular (outer dia, d_c), convergent (outer dia, $0.5d_c$), divergent (outer dia, $1.5d_c$), sudden contraction (outer dia, $0.5d_c$), and sudden expansion (outer dia, $1.5d_c$). In the second part of the study, parametric analysis with different divergence angles (CDA, ϕ) of the divergent chimney is performed. As the sloped ground absorber surface is also another significant parameter for controlling the performance of a SCPP, therefore, the third part of the study describes the impact of ground absorber surface slope (GSA,γ) on the SCPP performance. In the last part of the section, the ground sloped absorber with divergent chimney of the SCPP is considered for the study. Comparative study is made with different shapes of chimney, divergent chimney, sloped ground absorber, and sloped ground absorber surface along with the chimney divergence also. This analysis is carried out for as $\phi = -$

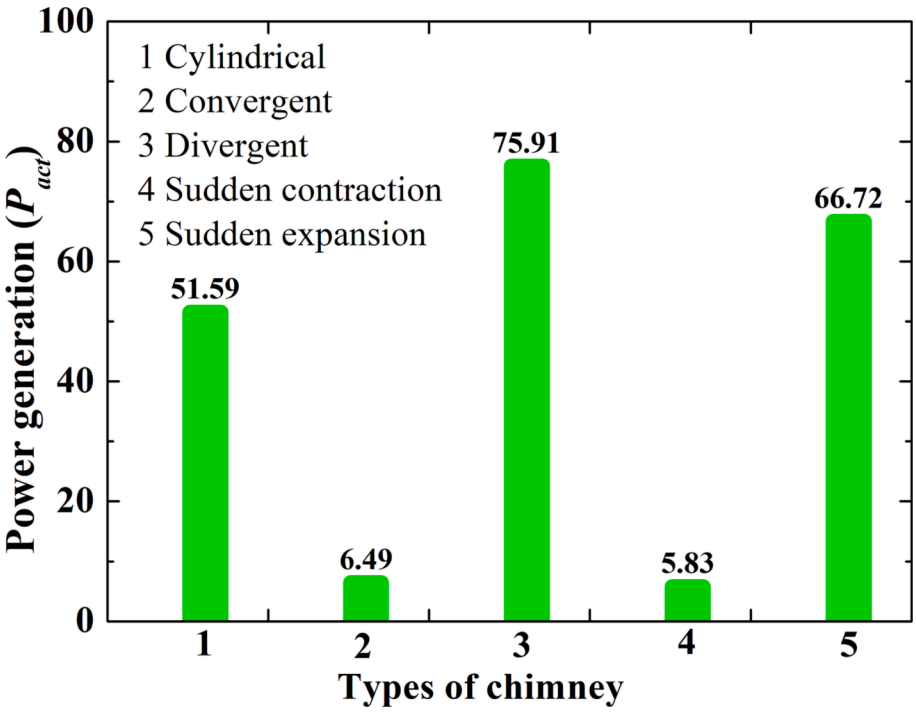

Fig. 13. Variation of actual power generation (P_{act}) with the cylindrical, convergent, divergent, sudden contraction, sudden expansion shaped chimneys.

0.75, 0, +0.75, 1.5, 2.25, 3.0° and γ = 0, 0.12, 0.24, 0.36, 0.48, 0.6°. The results are represented by pressure, temperature, mass flow rate, power, collector efficiency, and overall efficiency and measured the improvement of performance of Manzaranes plant..

4.1. Comparative assessment of the impact of chimney shape

The main aim of this section is to find out the best shape of a chimney towards obtaining a better performance of a SCPP. The considered shape are circular, convergent (outer dia, $0.5d_c$), divergent (outer dia, $1.5d_c$), sudden contraction (outer dia, $0.5d_c$), and sudden expansion (outer dia, $1.5d_c$). Here, the analysis is carried out based on the horizontal absorber surface ($\gamma = 0°$).

4.1.1. Effect of different shapes of chimneys on pressure, temperature, and velocity fields

In order to understand the flow-physics inside the SCPP, contours of static pressure, temperature, and velocity for the considered shapes of the chimney are presented in Figs. 8, 9, and 10 respectively. Since turbine is located at the chimney base, therefore, the zoom view of each figure has been shown at nearby chimney inlet zone. It is understood from the pressure contours (from Fig. 8), that the pressure values are minimum at the chimney wall for all the cases. The magnitude of pressure varies from −193 Pa to −7 Pa for the cylindrical chimney (Fig. 8a) i.e., -ve pressure throughout the total flow zone of SCPP. The maximum –ve pressure occurs at the wall near the chimney, the pressure rises when flow moves along the chimney. The variation of pressure for the convergent chimney (Fig. 8b) shows the drop in pressure inside SCPP is very less and the some chimney zone yields + ve pressure zone. The magnitude varies from −49 Pa to 54 Pa. this high-pressure zone occurs due to the nature of the shape of the chimney. It is clear, that less –ve pressure generation for convergent chimney enables less flow through the chimney. In the case of a divergent chimney (Fig. 8c), it reveals –ve pressure zone throughout the zone of SCPP similar to a cylindrical chimney while the magnitude of pressure drops more for this divergent chimney. This indicates high suction pressure (due to -ve value) at the chimney inlet zone due to divergent shape, the pressure varies from −246 Pa to −9Pa. The sudden contraction chimney (Fig. 8d) shows the variation of pressure from −231 Pa to 66 Pa. Some portion of the chimney occupies -ve pressure values and minimum pressure occurs at the sudden contraction location. The pressure near the chimney inlet becomes –ve but not too much in magnitude that yields less power generation in this case. For the sudden expansion-shaped chimney (Fig. 8e), pressure values vary from −236 Pa to −9 Pa, -ve value throughout the zone. The reduction of –ve pressure near the chimney is more relative to the cylindrical case, but lesser than in the divergent-shaped chimney.

The maximum temperature zone is noted at the ground wall (as shown in Fig. 9) from the temperature contours since the ground plate absorbs the energy. The temperature of the fluid at centre is more. The maximum temperature obtained for the cylindrical chimney (Fig. 9a) is 350 K, ~356 K for the convergent (Fig. 9b) and sudden contraction chimney (Fig. 9d), ~347 K for divergent (Fig. 9c) and sudden expansion (Fig. 9e) chimneys. More temperature rise for convergent and sudden contraction chimneys, which may be for the less mass flow rate through these cases and due to higher pressure. For the divergent and sudden expansion cases, as the mass flow rises, hence drops more temperature as observed. The velocity contours (as in Fig. 10) reveal zero velocity at the wall due to the no-slip condition; the velocity becomes maximum at the center near the chimney inlet. The magnitude of chimney base velocity is noted for the chimney with cylindrical (~17 m/s), convergent (~6 m/s), divergent (~19 m/s), sudden contraction (~6 m/s), and sudden expansion (18 m/s) shape, respectively. The maximum velocity of 21 m/s is noted for the sudden contraction-shaped chimney at the contraction zone. Certain increment of chimney base velocity is revealed for divergent and sudden expansion cases of chimneys compared to the cylindrical cases (Manzaranes) SCPP, which is referred to as the base.

4.1.2. Effect of different shaped chimneys on the variations of CB pressure, CB velocity, and CB temperature

The feasibility study of an SCPP requires in-depth knowledge of the local variation of pressure, temperature, and velocity, especially at the chimney base for obtaining the performance parameters. Fig. 11 shows all these local variations for the different circular (outer dia, d_c),

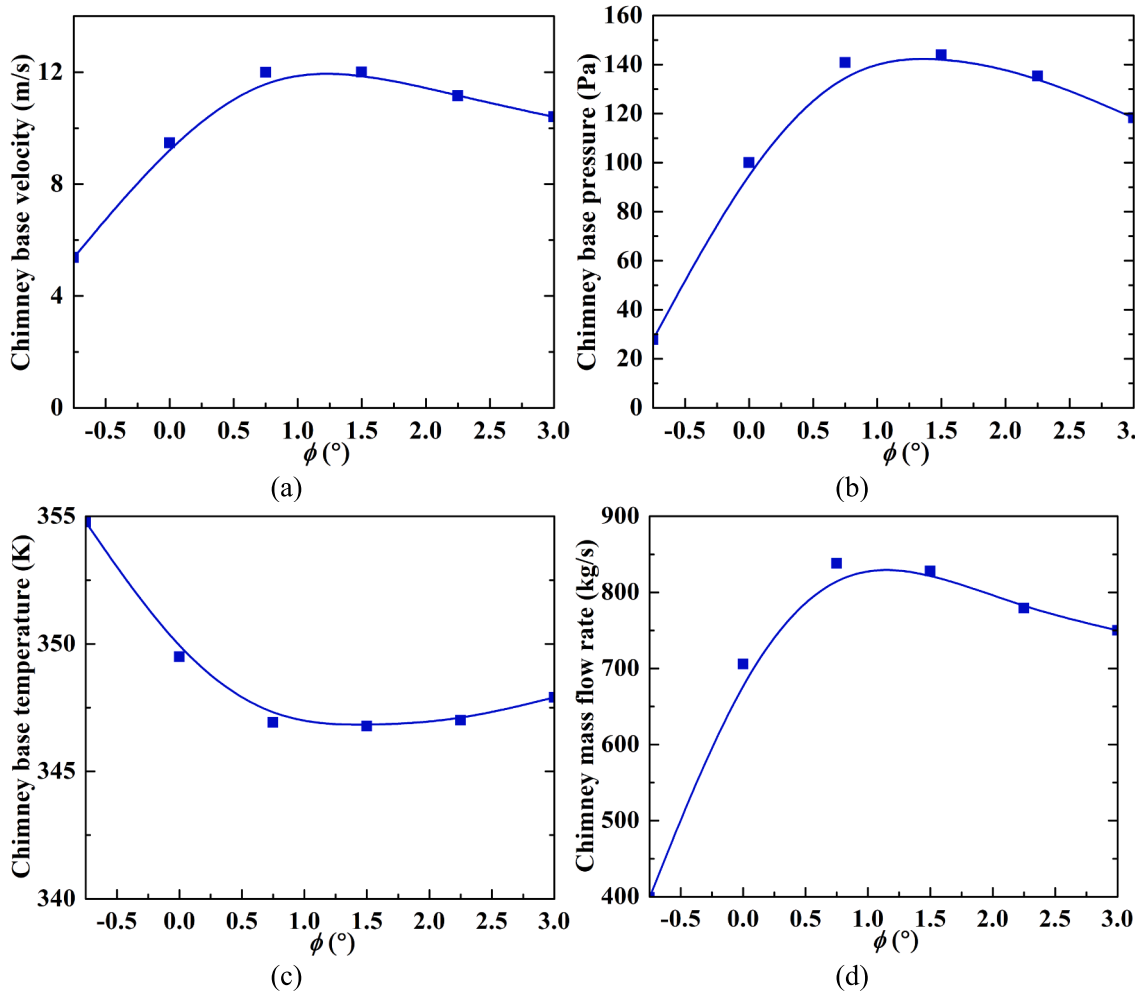

Fig. 14. Variation of chimney base (a) pressure, (b) velocity, (c) temperature, and (d) mass flow rate through the different divergence angle (ϕ) of the chimneys when $\gamma = 0^{\circ}$.

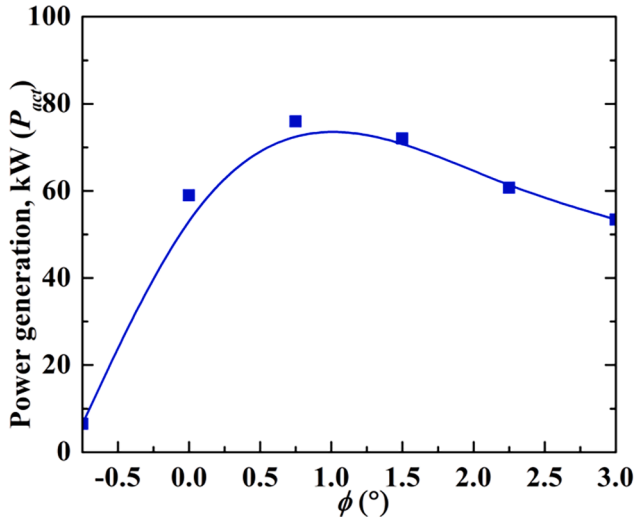

Fig. 15. Variation of actual power generation (P_{act}) for the different divergence angles (ϕ) of the chimney when $\gamma = 0^{\circ}$.

convergent (outer dia, $0.5d_c$), divergent (outer dia, $1.5d_c$), sudden contraction (outer dia, $0.5d_c$) and sudden expansion (outer dia, $1.5d_c$) models of the modified SCPP. It is depicted from the pressure variations (Fig. 11a), at the chimney base, that the pressure line for the cylindrical chimney lies in between convergent/ sudden contraction and divergent/ sudden expansion. No significant variation in pressure is noted for the convergent or sudden contraction, divergent or sudden expansion shaped chimneys. The pressure magnitude is minimum at the wall as depicted from the pressure contour plots (Fig. 8). The higher pressure is noted for the convergent and sudden contraction cases while there are very less for divergent and sudden expansion cases. In the case of velocity profiles (Fig. 11b), it is noted that the velocity curves are having lower value for the sudden contraction and convergent shaped chimneys, whereas it becomes higher in magnitude for the divergent or sudden expansion shaped chimney. The velocity of the cylindrical chimney lies in the middle with a higher gain in velocity like divergent or sudden expansion. The temperature magnitude variation (Fig. 11c) curves show the minimum temperature for cylindrical, divergent, and sudden expansion cases of chimneys. The higher temperature magnitude for the convergent or sudden contraction is owing to the lower velocity at this zone.

4.1.3. Effect of different shaped chimneys on average chimney pressure and velocity

The averaging effect of pressure and velocity may not be clear from the aforesaid discussion. Hence, this section illustrates the average pressure and average velocity, which are required for calculating power output from the SCPP. Fig. 12 depicts the chimney base pressure and velocity for the circular (outer dia, d_c), convergent (outer dia, $0.5d_c$),

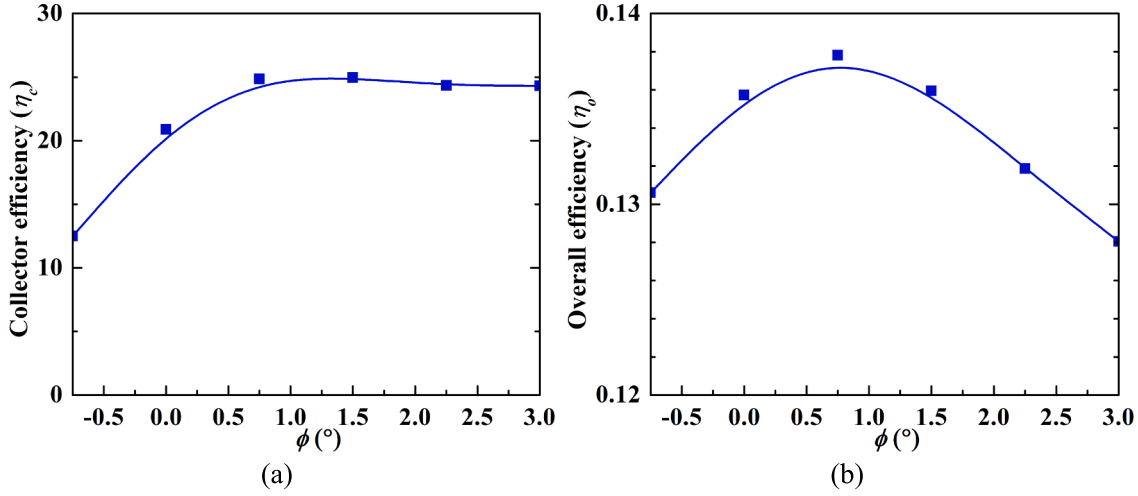

Fig. 16. Variation of (a) collector efficiency (η_c), and (b) overall efficiency (η_o) for the different divergence angle (ϕ) of the chimneys when $\gamma = 0^{\circ}$.

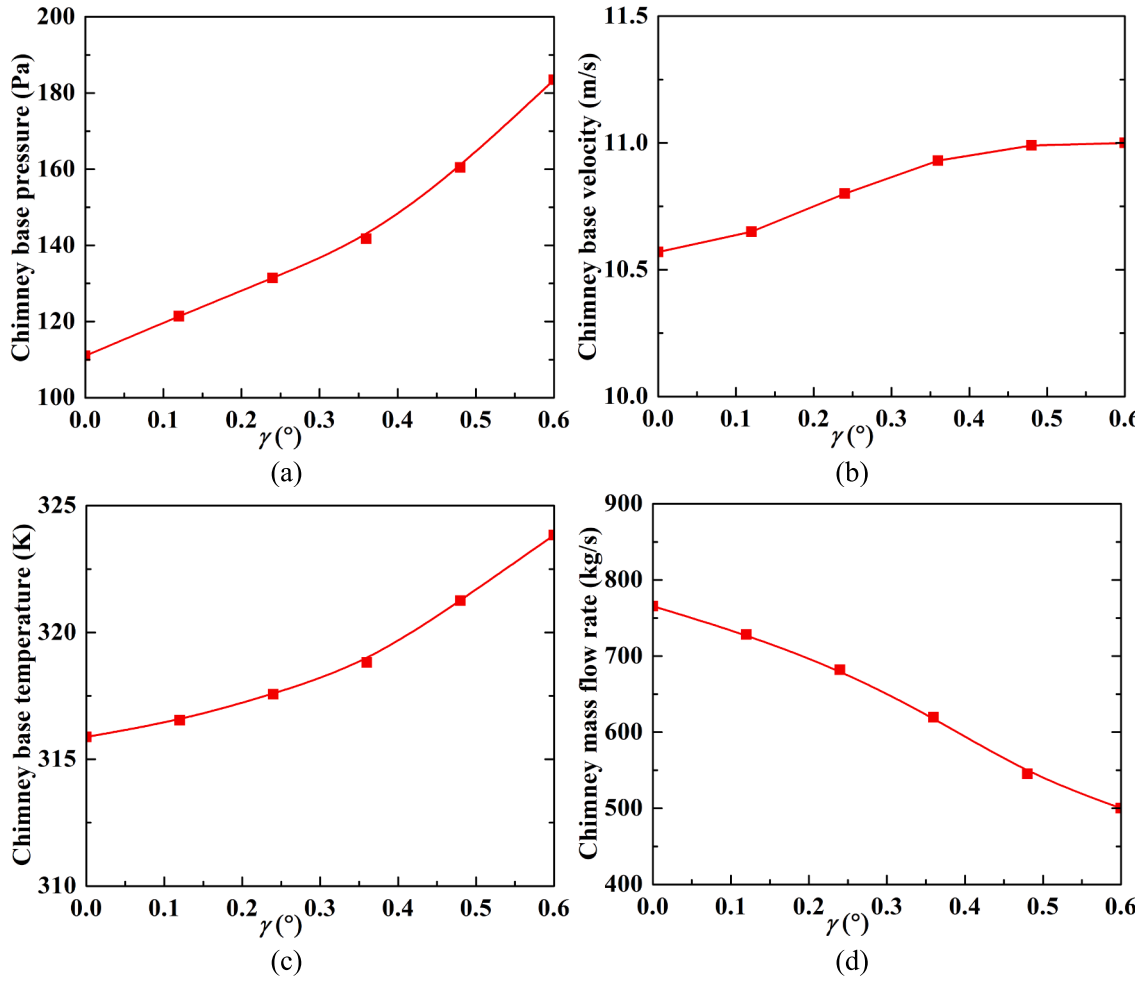

Fig. 17. Variation of chimney base (a) pressure, (b) velocity, (c) temperature, and (d) mass flow rate through the different ground slope angle GSA (γ) when $\phi = 0^{\circ}$.

divergent (outer dia, $1.5d_c$), sudden contraction (outer dia, $0.5d_c$) and sudden expansion (outer dia, $1.5d_c$) models. The magnitude of minimum pressure values is 111 Pa, 27.81 Pa, 145.77 Pa, 21.8 Pa, and 39.64 Pa (actually all are in –ve values) for circular, convergent, divergent, sudden contraction, and sudden expansion chimneys respectively. Maximum minimum pressure is reported for the divergent chimney. Both the divergent and sudden expansion cases predict better performance relative to the cylindrical case (base case), while convergent or sudden expansion cases show a very poor drop in pressure. The measured gain in pressure for the divergent chimney is 31%, and the sudden expansion chimney is 26% compared to the cylindrical-shaped chimney (base case). The chimney base velocity reveals a rise in

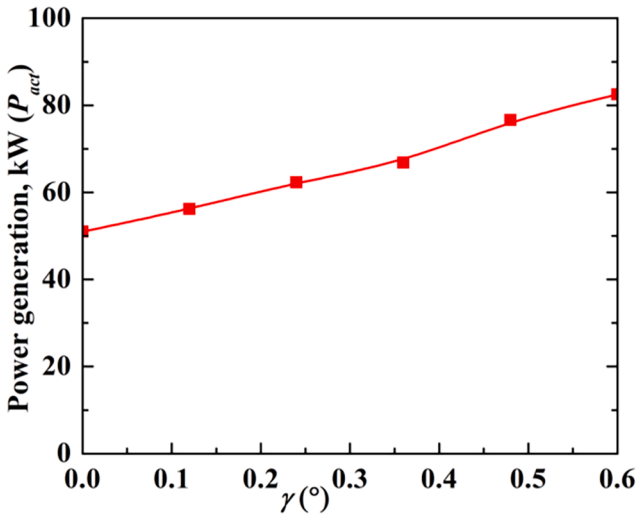

Fig. 18. Variation of actual power generation (P_{act}) through the different slopes of the ground absorber surface (γ) when $\phi = 0^{\circ}$.

velocity for divergent and sudden expansion compared to the base case, while the velocity is less for convergent and sudden contraction in both cases. The gain in velocity is about 12% for divergent cases, and 4% for sudden expansion cases relative to ref. base case of a cylindrical chimney.

4.1.4. Effect of different shaped chimneys on power

Finally, the effect of fluid pressure and velocity is reflected by the power generated by the SCPP, which is calculated and presented in Fig. 13 for the different shaped chimneys of the modified SCPP. The magnitude of power generation is about ~ 51.5, 6.49, 75.97, 5.82, and 66.71 kW for the circular, convergent, divergent, sudden contraction, and sudden expansion chimneys, respectively. This is clearly revealed that the power generation could be enhanced markedly by adopting the divergent or sudden expansion-shaped chimneys both, while the maximum power is obtained with the divergent cases. The gain in the power generation is 47% for the divergent chimney, and 31% for the sudden expansion-shaped chimney relative to the cylindrical reference chimney case.

4.2. Impact of chimney divergence

The aforesaid discussions clearly depict the substantial improvement in the conventional SCPP performance by using divergent or sudden expansion-shaped chimneys instead of the cylindrical chimney (when $\phi = 0^{\circ}$). Both the shape of the chimneys are beneficial for enhancing power generation. However, more power is generated by the divergent-shaped chimney. Therefore, to find out further improvement, if any, on the power generation, the effect of the chimney divergence angle (CDA) is assessed meticulously.

4.2.1. Effect of divergent chimneys on CB pressure, CB velocity, CB temperature, and mass flow rate

It is pertinent to mention that, the study of the divergent chimney is a similar study of flow through a converging–diverging nozzle, where the chimney base is the throat. Due to nozzle action, pressure at the throat may decrease. Fig. 14 shows the variation of average pressure, velocity, temperature, and mass flow rate at the chimney base for the varying CDA, $\phi = -0.75,\ 0,\ +0.75,\ 1.5,\ 2.25,\ 3.0^{\circ}$. It is understood that average pressure values decrease (pressure values are actually –ve) with increasing CDA (from -0.75° to $+\ 0.75^{\circ}$) as shown in Fig. 14(a). The enhancement of suction pressure at the throat yields a remarkable rise in the mass flow rate of air that in turn lessens the air temperature. Air velocity rises due to the same effect in the divergent geometry also. The chimney base pressure rises with further increasing CDA (after $+\ 0.75^{\circ}$). This is due to the loss of fluid viscous effect. This decreases the average velocity and mass flow rate as shown in Fig. 14(b and d). A decrease in mass flow rate increases the air temperature (as shown in Fig. 14c). In every case of the parametric study, it is understood that the optimum value of CDA of $\phi = +0.75^{\circ}$.

4.2.2. Effect of divergent chimneys on power

The influence of CDA on power generation is the function of average pressure and velocity. The power generation by the modified SCPP with the varying CDA is presented in Fig. 15. As the average pressure and velocity are maximum at CDA $\phi = +0.75^{\circ}$, hence the power is maximum at this divergent angle, its value 76 kW. Further rise or drop in CDA lessens the power generation. So, optimum divergence angle (ϕ) is obtained for the maximum power generation. This is an important finding of this study. Maximum gain in power is 47% relative to base case.

4.2.3. Effect of divergent chimneys on efficiencies

Two efficiencies collector efficiency (η_c) and overall efficiency (η_o) are chosen for the discussion of the performance analysis of the modified SCPP. The collector efficiency (η_c) depends on the mass flow rate and temperature rise of air and overall efficiency (η_o) depends on the power generation, since the collector area, and solar intensity remains constant throughout the study. From the variation of efficiencies (as illustrated in Fig. 16) with CDA, it is noted that η_c rises first then no notable change in the efficiency, while η_o occurs an optimum value (which is, CDA of $+\ 0.75^{\circ}$) as maximum power available there.

4.3. Impact of ground slope

From the previous subsection, it is clearly observed that the efficacy

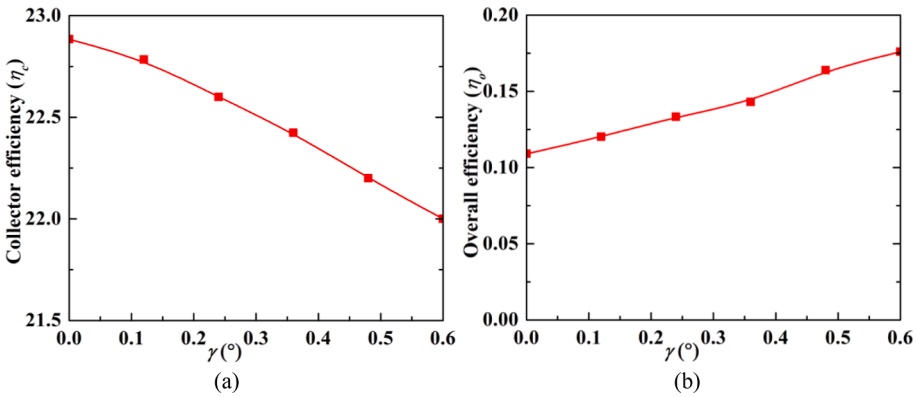

Fig. 19. Variation of (a) collector efficiency (η_c), (b) overall efficiency (η_o) for the different angles of the ground absorber surface when $\phi = 0^{\circ}$.

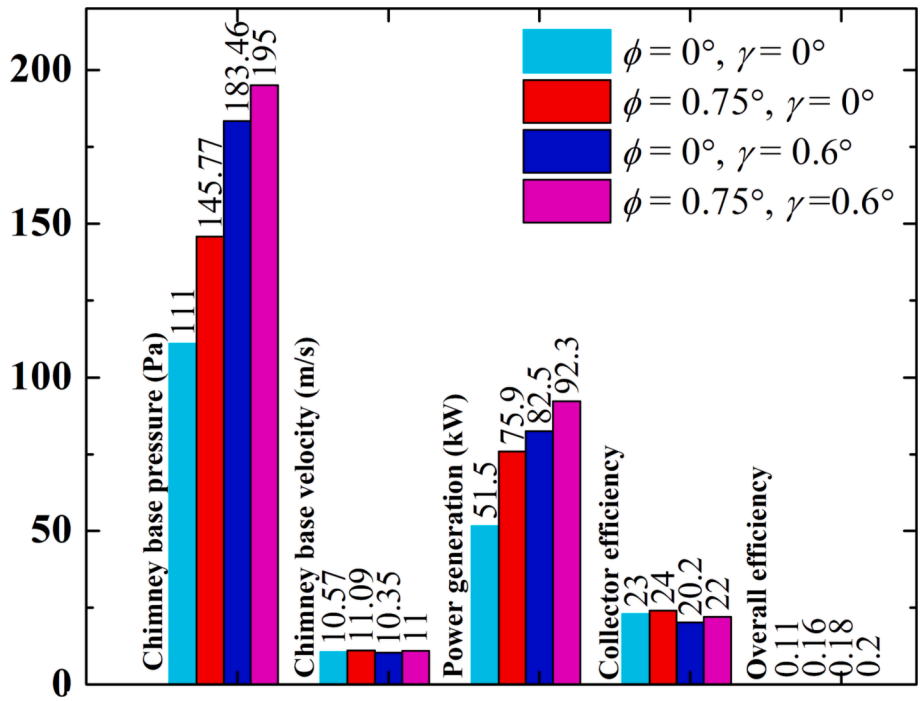

Fig. 20. Variation of chimney base pressure, velocity, power generation, collector efficacy, and overall efficiency for the modified SCPP combining ground sloped divergent chimney.

Table 5
Improvement in power generation and pressure compared to conventional SCPP (Manzaranes plant).

Criteria	$\phi = 0^{\circ}$, $\gamma = 0^{\circ}$	$\phi = +0.75^{\circ}$, $\gamma = 0^{\circ}$	$\phi = 0^{\circ}$, $\gamma = 0.6^{\circ}$	$\phi = 0.75^{\circ}$, $\gamma = 0.6^{\circ}$
Chimney base pressure (Pa)	111.00	145.77	183.46	195.00
% increase	0.00	31.32	65.28	75.68
Power generation (P_{act}) kW	51.50	75.90	82.50	92.30
% increase	0.00	47.38	60.19	79.22

of the conventional SCPP could be improved substantially by adopting the divergent chimney over the cylindrical chimney. In this section, a further attempt has been taken to enhance the SCPP performance by incorporating the sloped ground absorber surface instead of the horizontal surface ($\gamma = 0^{\circ}$). Before using the divergent chimney in a conventional SCPP, it is essential to know the optimum ground slope angle (GSA,γ) for cylindrical chimney. To do this, the flow and performance analyses are carried out for GSA, $\gamma(= 0^0$ for horizontal ground case), 0. 12, 0.24, 0.36, 0.48, 0.6° in Manzaranes plant.

4.3.1. *Effect of ground slope on chimney base pressure, velocity, temperature, and mass flow rate*

Flow parameters are explained for the considered range of GSA (γ = 0, 0.12, 0.24, 0.36, 0.48, 0.6°) to depict the chimney base pressure, velocity, temperature, and mass flow rate, which are demonstrated in Fig. 17. The analysis revealed that the chimney base pressure drops with the rising GSA (pressure value actually –ve), however mass flow rate does not rise. The reason for lessening the mass flow rate is due to the reduction of the throat area as well as rise in temperature. The rise in temperature with the increasing GSA yields a drop in fluid density. The rise in the velocity with the increasing GSA does not influence the mass flow rate. It is to be noted for the divergent chimney, mass flow rate increases as pressure drops, suction action rise due to divergence of the chimney, that yields drop in the air temperature markedly.

4.3.2. *Effect of ground slope on power*

The power generation with increasing GSA (as in Fig. 18) shows an improvement of power generation always for rising GSA (γ). The maximum power generation is noted at GSA of 0.6° (for the present case) of 80 kW. This gain in power generation compared to the base model (γ = 0°) is 60%. There is no optimum value as chimney base pressure and velocity both rise with GSA. This is also an important finding of this study. It is to be mentioned that gain in the power generation is ~ 45% for the divergent chimney.

4.3.3. *Effect of ground absorber slope on different efficiencies*

Here in Fig. 19, the collector efficiency (η_c) drops and overall efficiency (η_o) rises with a rise in GSA(γ). The dropping trend in the collector efficiency is due to mainly for the reduction of working fluid mass flow rate, while the increase in power generation is due to the increase in overall efficiency (η_o). Here it is also noted that the collector efficiency

Table 6
Regression coefficients (b_1 to b_6) for the power generation (P_{act}), collector efficiency (η_c) and overall efficiency (η_o), and mass flow rate (m_a).

		P_{act}	η_c	η_o	m_a
Coefficients	b_1	51.103353120285881	22.642722139516874	0.133430302402937	747.4169617475849
	b_2	25.920860969183590	3.057924700594755	0.003884271014938	135.6185412128146
	b_3	9.174390705685724	0.492877347988450	−0.044006571630737	−217.0705481221446
	b_4	−12.30866486740432	−4.348864824623891	0.042581891706241	1.0000000000000
	b_5	−8.565112585165810	−0.875910033487072	−0.001940894628548	−046.2158247190077
	b_6	23.078171526622924	−2.728343080107603	0.199973164652932	−354.1076566679185

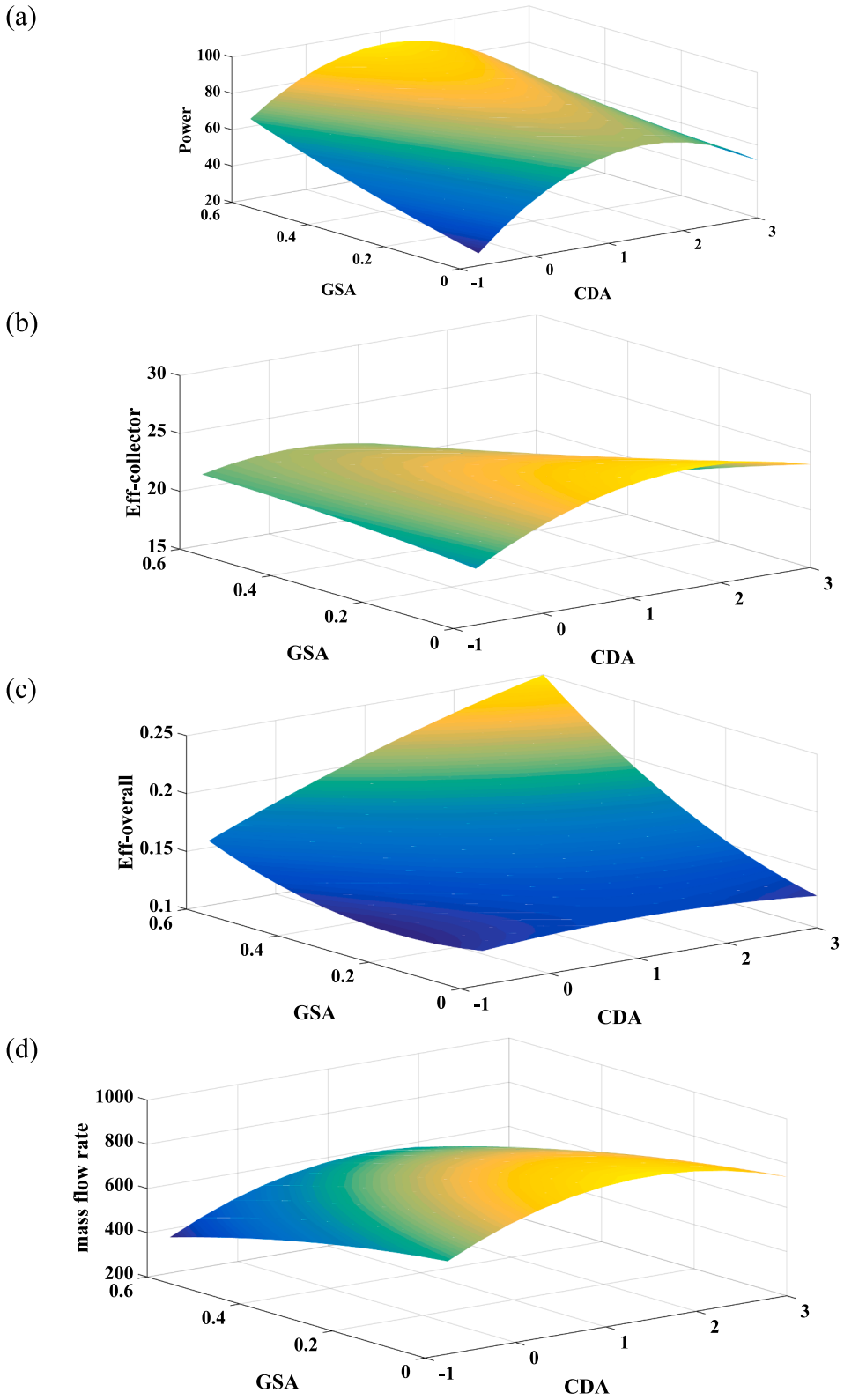

Fig. 21. Surface plot for (a) actual power (P_{act}), (b) collector efficiency (P_{act}), (c) overall efficiency (P_{act}), and (d) mass flow rate (P_{act}) for the modified SCPP with both chimney divergence and sloped ground absorber surface.

(η_c) rises for the increasing CDA (ϕ) and it occurs at an optimum value.

4.4. Impact of ground sloped divergent chimney SCPP

Finally, the SCPP is modeled by adopting the better sloped ground absorber (γ) and optimum divergent chimney (ϕ) SCPP. For the extensive analysis of the flow field and performance, the ground slope angle GSA, $\gamma = 0.6^{\circ}$, and chimney divergence angle CDA, $\phi = 0.75^{\circ}$ are used.

4.4.1. Effect of ground sloped divergent chimney on chimney base pressure, velocity, power, collector efficacy, and overall efficiency

The effect of ground absorber surface slope (γ) and chimney divergence (ϕ) on the base pressure, velocity, power, collector efficiency, and overall efficiency are illustrated in Fig. 20. The analysis is compared with the results of base case ($\phi = 0^{\circ}, \gamma = 0^{\circ}$), divergent chimney ($\phi = +0.75^{\circ}$, $\gamma = 0^{\circ}$), the ground sloped SCPP ($\phi = 0^{\circ}$, $\gamma = 0.6^{\circ}$) with the ground sloped divergent chimney ($\phi = 0.75^{\circ}$, $\gamma = 0.6^{\circ}$) SCPP. From the comparative analysis, no noticeable variation is noted for the chimney base velocity, collector efficiency, and overall efficiency. Chimney base pressure drops more with the magnitude of 194 Pa which is 75% gain compared to the base case, 6% gain compared to the ground sloped case, 33% gain compared to the divergent chimney model. Improvement in this geometry of power generation is 92 kW, which is 80% more relative to the base case, 12% more than the slopped ground case, and 21% more than the divergent chimney case. The gain in power generation and gain in pressure compared to the base Manzaranes plant is shown in Table 5.

4.5. Regression analysis

This section develops mathematical correlations to find out the actual power generation (P_{act}), collector efficiency (η_c) and overall efficiency (η_o), and mass flow rate (m_a) as a function of CDA (ϕ) and GSA (γ). This will help to predict any intermediate output data point, which will be very helpful for the designer. It is useful to find out the outputs easily by the mathematical correlations with the different CDA and GSA. The mathematical correlations are developed through the regression analysis using MATLAB written code. The developed correlations are expressed in Eqs. (14) to (17). The respective regression coefficients (b_1 to b_6) are listed in Table 6. Utilizing the mathematical correlations, a three-dimensional surface plot for the power generation (P_{act}), collector efficiency (η_c) and overall efficiency (η_o), and mass flow rate (m_a) is generated as a function of CDA (ϕ) and GSA (γ), which are shown in Fig. 21. Fig. 21 (a) illustrates that actual power generation, it rises with the increasing GSA, and it has an optimum value for the varying CDA. The variation of collector efficiency (Fig. 21b), the efficiency drops with GSA, while it increases with the CDA up to some level, the change in the magnitude is very small. Fig. 21(c) shows the enhancement of the overall efficiency with GSA, while the efficiency has an optimum value with rising CDA. The mass flow rate surface plot (Fig. 21d) reveals the decrease in mass flow with rising GSA, but with CDA, optimum CDA exists in obtaining maximum mass flow rate.

$$P_{act} = b_1 + b_2\varphi + b_3\gamma + b_4\varphi\gamma + b_5\varphi^2 + b_6\gamma^2 \quad (14)$$

$$\eta_c = b_1 + b_2\varphi + b_3\gamma + b_4\varphi\gamma + b_5\varphi^2 + b_6\gamma^2 \quad (15)$$

$$\eta_o = b_1 + b_2\varphi + b_3\gamma + b_4\varphi\gamma + b_5\varphi^2 + b_6\gamma^2 \quad (16)$$

$$m_a = b_1 + b_2\varphi + b_3\gamma + b_4\varphi\gamma + b_5\varphi^2 + b_6\gamma^2 \quad (17)$$

5. Conclusion

In this study, an attempt has been made to maximize the thermal performance and the power generation by modifying the classical SCPP adopting the chimney shape with the ground sloped absorber. The parametric analysis with angles of the different chimney divergence (CDA, φ) and the impact of ground slope angle (GSA, γ) on the SCPP performance is also scrutinized. Finally, the ground-sloped divergent chimney SCPP is selected for maximizing the performance. The comparison is made with the reference case, divergent chimney, and sloped ground and finally the improvement by using sloped ground divergent chimney SCPP. Assessments are carried out through pressure, temperature, mass flow rate, power generation, collector efficiency, and overall efficiency. The major finding is summarized below:

- Chimneys with divergence or sudden expansion shape as well as sloped ground absorber are beneficial for enhancing the performance of a classical SCPP.
- With the divergent chimney, the optimum divergence angle (CDA) is $\phi = +0.75^{\circ}$, this yields maximum power of ~ 76 kW (47% gain), maximum efficiency (0.136%), and minimum pressure (145.77 Pa). An increase or decrease in CDA lessens the power generation while the chimney with sudden expansion (with outer dia = $1.5d_c$) power generation up to ~ 31% (65 kW) with horizontal ground absorber surface.
- Converging or sudden contraction geometry has no beneficial impact for improving the performance of an SCPP.
- There is no optimum GSA in achieving power generation. More GSA enhances the power and overall efficiency.
- With a sloped ground absorber angle $\gamma = 0.6^{\circ}$, the gain in power generation is 60% (82 kW) relative to base case.
- The combination of ground sloped absorber ($\gamma = 0.6^{\circ}$) and divergent chimney ($\phi = +0.75^{\circ}$) enhances the power generation up to 80% (92 kW) more than the classical Manzaranes plant.

Declaration of Competing Interest

The authors declare that they have no known competing financial interests or personal relationships that could have appeared to influence the work reported in this paper.

Acknowledgement

Supported by the central publication fund of Hochschule Düsseldorf University of Applied Sciences.

References

[1] Abdelmohimen MAH, Algarni SA. Numerical investigation of solar chimney power plants performance for Saudi Arabia weather conditions. Sust Cities Soc 2018;38:1–8.
[2] Ansys Inc, (2016), ANSYS Fluent 16 Theory guide.
[3] Attig-Bahar F, Sahraoui M, Guellouz MS, Kaddeche S. Effect of the ground heat storage on solar chimney power plant performance in the South of Tunisia: Case of Tozeur. Sol Energy 2019;193:545–55.
[4] Bhattacharyya S, Chattopadhyay H, Benim AC. Heat transfer enhancement of laminar flow of ethylene glycol through a square channel fitted with angular cut wavy strip. Procedia Eng 2016;157:19–28.
[5] Biswas N, Manna NK, Datta A, Mandal DK, Benim AC. Role of aspiration to enhance MHD convection in protruded heater cavity. Prog Comput Fluid Dyn 2020;20(6):363–78.
[6] Cao F, Li H, Zhang Y, Zhao L. Numerical simulation and comparison of conventional and sloped solar chimney power plants: the case for Lanzhou. Sci World J 2013;852864:1–8.
[7] Chakravarty A, Biswas N, Ghosh K, Manna NK, Mukhopadhyay A, Sen S. Impact of side injection on heat removal from truncated conical heat-generating porous bed: thermal non-equilibrium approach. J Thermal Anal Calorim 2021;143:3741–60.
[8] Chitsomboon T. The effect of chimney-top convergence on efficiency of a solar chimney. thailand.Int J Renew Energ Eng 2001;3(2):339e46.
[9] Cuce E, Sen H, Cuce PM. Numerical performance modelling of solar chimney power plants: Influence of chimney height for a pilot plant in Manzanares, Spain. Sus Energy Technol Assess 2020;39.
[10] Cuce E. Güneş bacası güç santrallerinde toplayıcı eğiminin çıkış gücüne ve sistem verimine etkisi. Uludağ Üniversitesi Mühendislik Fakültesi Dergisi 2020;25(2):1025–38.
[11] Cuce PM, Cuce E, Sen H. Improving electricity production in Solar chimney power plnats with sloping ground design: An extensive CFD research. J Sol Energy Res Updates 2020;7:122–31.
[12] Cuce E, Cuce PM, Sen H, Sudhakar K, Berardi U, Serencam U. Impacts of ground slope on main performance figures of solar chimney power plants: a comprehensive CFD research with experimental validation. Int J Photoenergy 2021;6612222:1–11.
[13] Cuce E, Saxena A, Cuce PM, Harun S, Shaopeng G, Sudhakar K. Performance assessment of solar chimney power plants with the impacts of divergent and convergent chimney geometry. Int J Low-Carbon Technol 2021;16:704–14.
[14] Das P, Chandramohan VP. Computational study on the effect of collector cover inclination angle, absorber plate diameter and chimney height on flow and performance parameters of solar updraft tower (SUT) plant. Energy 2019;172:366–79.

[15] Das P, Chandramohan VP. 3D numerical study on estimating flow and performance parameters of solar updraft tower (SUT) plat:impact of divergent angle of chimney, ambient temperature, solar flux and turbine efficiency. J Clear Prod 2020;256.
[16] Das P, Chandramohan VP. A review on solar updraft tower plant technology: Thermodynamic analysis, worldwide status, recent advances, major challenges and opportunities. Sust Energy Technol Assess 2022;52.
[17] Elwekeel FNM, Abdala AMM, Rahman MM. Effects of novel collector roof on solar chimney power plant performance. J Sol Energy Engg 2019;141.
[18] Fard KP, Beheshti PH. Performance enhancement and environmental impact analysis of a solar chimney power plant: Twenty-four-hour simulation in climate condition of isfahan province Iran. Int J Eng 2017;30:1260–9.
[19] Fallah SH, Valipour MS. Evaluation of Solar chimney power plant performance: The effect of artificial roughness of collector. Sol Energy 2019;188:175–84.
[20] Gholamalizadeh E, Chung JD. Analysis of fluid flow and heat transfer on a solar updraft tower power plant coupled with a wind turbine using computational fluid dynamics. Appl Therm Engg 2017;126:548–58.
[21] Gholamalizadeh E, Kim MH. CFD (computational fluid dynamics) analysis of a solar-chimney power plant with inclined collector roof. Energy 2016;107:661–7.
[22] Guo P, Li J, Wang Y. Numerical simulations of solar chimney power plant with radiation model. Ren Energy 2014;62:24–30.
[23] Haaf W, Friedrich K, Mayr G, Schlaich J. Solar chimneys part I: principle and construction of the pilot plant in manzanares. Int J Sol Energy 1983;2(1):3–20.
[24] Haaf W. Solar chimneys part II: preliminary test results from the manzanares pilot plant. Int J Sol Energy 1984;2(2):141–61.
[25] Hassan A, Ali M, Waqas A. Numerical investigation on performance of solar chimney power plant by varying collector slope and chimney diverging angle. Energy 2018;142:411–25.
[26] Huang H, Zhang H, Huang Y, Lu F. Simulation calculation on solar chimney power plant system. challenges of power engineering and environment. Springer; 2007. p. 1158–61.
[27] Kasaeian A, Ghalamchi M, Ghalamchi M. Simulation and optimization of geometric parameters of a solar chimney in Tehran. Energy Conv Manage 2014;83:28–34.
[28] Keshari SR, Chandramohan VP, Das P. A 3D numerical study to evaluate optimum collector inclination angle of Manzanares solar updraft tower power plant. Sol Energy 2021;226:455–67.
[29] Koonsrisuk A, Chitsomboon T. Effects of flow area changes on the potential of solar chimney power plants. Energy 2013;51:400–6.
[30] Li J, Guo H, Huang S. Power generation quality analysis and geometric optimization for solar chimney power plants. Sol Energy 2016;139:228–37.
[31] Li JY, Guo PH, Wang Y. Effects of collector radius and chimney height on power output of a solar chimney power plant with turbines. Ren Energy 2012;47:21–8.
[32] Mandal DK, Goswami P, Pradhan S, Chakraborty R, Khan NA, Bose P. A numerical experimentation on fluid flow and heat transfer in a SCPP. IOP Conf Series: Mater Sci Engg 2021;1080(1).
[33] Mandal DK, Pradhan S, Chakraborty R, Barman A, Biswas N. Experimental investigation of a solar chimney power plant and its numerical verification of thermo-physical flow parameters for performance enhancement. Sus Energy Technol Assess 2022;50:101786.
[34] Santra S, Mandal DK, Chakrabarti S. Effect of pulsatile blood flow on LDL transport in arterial layers. Prog Comp Fluid Dyn 2018;18(3):177–87.
[35] Okada S, Uchida T, Karasudani, Tand Ohya Y. Improvement in solar chimney power generation by using a diffuser tower. J Sol. Energy Eng. 2015;137. 031009 – 1.
[36] Praveen V, Das P, Chadromohan VP. A novel concept of introducing a fillet at the chimney base of solar updraft tower plant and thereby improving the performance: A numerical study. Rene 2021;179:37–46.
[37] Patel SK, Prasad D, Ahmed MR. Computational studies on the effect ofgeometric parameters on the performance of a solar chimney power plant. Energy Conv Manage 2014;77:424–31.
[38] Padki MM, Sherif SA. On a simple analytical model for solar chimneys. Int J Energ Res 1999;349:345–9.
[39] Pradhan S, Chakraborty R, Mandal DK, Barman A, Bose P. Design and performance analysis of solar chimney power plant (SCPP): a Review. Sus Energy Technol Assess 2021;47.
[40] Rabehi R, Chaker A, Aouachria Z, Tingzhen M. CFD analysis on the performance of a solar chimney power plant system: Case study in Algeria. Int J Green Energy 2017;14:971–82.
[41] Sangi R, Amidpour M, Hosseinizadeh B. Modeling and numerical simulation of solar chimney power plants. Sol Energy 2011;85:829–38.
[42] Senbeto M. Numerical simulations of solar chimney power plant with thermal storage. Int J Engg Res Technol 2020;9(10):103–6.
[43] Schlaich JR, Bergermann R, Schiel W, Weinrebe G. Design of commercial solar updraft tower systems—utilization of solar induced convective flows for power generation. J Sol Energy Engg 2005;127(1):117–24.
[44] Shahi DVV, Gupta A, Nayak VS. CFD analysis of solar chimney wind power plant by Ansys Fluent. Int J Technol Res Engg 2018;5(9):3746–51.
[45] Sudprasert S, Chinsorranant C, Rattanadecho P. Numerical study of vertical Solar chimneys with moist air in a hot and humid climate. Int J Heat Mass Transf 2016; 102:645–56.
[46] Tayebi T, Djezzar M. Numerical simulation of natural convection in a solar chimney. Int J Renew Energy Res 2012;2(4):712–7.
[47] Tayebi T, Djezzar M. Numerical analysis of flows in a solar chimney power plant with a curved junction. Int J Energy Sci (IJES) 2013;3 I(4):280–6.
[48] Tayebi T, Djezzar M. Effect of varying ambient temperature and solar radiation on the flow in a solar chimney collector. Int J Smart Grid Clean Energy 2016;5(1): 16–23.
[49] Tayebi T. Entropy generation analysis of convective airflow in a solar updraft tower power plant. Heat transfer-Asian Research 2019;48(8):3885–901.
[50] Von Backström TW, Gannon AJ. Comprehensive flow through solar power plant chimneys. J Solar Energy-T ASME 2000;122(3):138–45.
[51] Zhou X, Yang J, Xiao B, Hou G, Xing F. Analysis of chimney height for solar chimney power plant. Appl Therm Engg 2008;29(1):178–85.

Dipak Kumar Mandal graduated in Mechanical Engineering from the Institution of Engineers, in 1997. He received his Master"s degree from the IIEST, Shibpur, in 1999. He completed his PhD from same university in 2010. His research areas are CFD, heat transfer, porus body, bio fluid mechanics, etc. He wrote two books, Fluid Mechanics and Hydraulic Machines, published by Vikash Publishing House Pvt. Ltd., and Power Plant Engineering: Theory and Practice by Wiley India Pvt. Ltd. He has worked in the thermal power plant for 12 years. Presently, he is working as an Associate Professor at the College of Engineering and Management, Kolaghat. He has published a good number of research papers in international journals and conference proceedings. He is a life member of the IEI.

Nirmalendu Biswas graduated from Jadavpur University and did Master's in Mechanical Engineering from Jadavpur University. He received his Ph.D. in Engineering from Jadavpur University, Kolkata in 2016. He has more than ten years of industrial experience. Presently he is an Assistant Professor in the Department of Power Engineering, Jadavpur University, Kolkata, India since 2019. His research interests include heat transfer, microfluidics, multiphase-flow, energy storage, phase-change material, bio-fluid mechanics, and others. He has published a good number of research papers in international journals and conference proceedings. He in an INAE fellow recipient. He is a life member of the ISHMT and IEI.

Nirmal K. Manna completed Ph.D. (Mechanical Engineering) from Jadavpur University in 2005, Master's (Heat Power) from Bengal Engineering Deemed University (presently know as Indian Institute of Engineering Science and Technology) in 1996. He has 4 years of industrial experience and has been working as professor in the Mechanical Engineering Department of Jadavpur University in India since 2007. His research interests are development of CFD code on single and multiphase flows, bio-fluid mechanics, free and forced convection, spool valve of HCS, FCI, and premixing. He has published a good number of research papers in international journals and conference proceedings.

Ali Cemal Benim received his B.Sc. and M.Sc. degrees in Mechanical Engineering at the Boğaziçi University, Istanbul, Turkey. He received his Ph.D. degree at the University of Stuttgart, Germany, in 1988, on the topic "Finite Element Modeling of Turbulent Diffusion Flames" with "Degree of Distinction". Following a post-doctoral period at the University of Stuttgart, in 1990 he joined ABB Turbo Systems Ltd. in Baden, Switzerland, where he was the manager of the "Computational Flow and Combustion Modeling" group. Since January 1996, he is Professor for Energy Technology and Head of Center of Flow Simulation at the Duesseldorf University of Applied Sciences, Duesseldorf, Germany.